JCI The Journal of Clinical Investigation

Endoplasmic reticulum-associated degradation is required for nephrin maturation and kidney glomerular filtration function

Sei Yoshida, … , Markus Bitzer, Ling Qi

J Clin Invest. 2021. https://doi.org/10.1172/JCI143988.

Research In-Press Preview Cell biology Nephrology

Graphical abstract

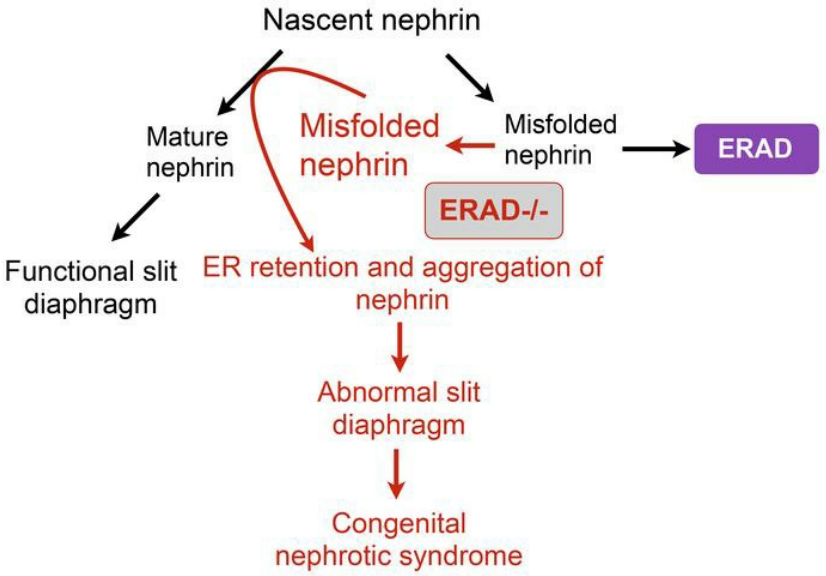

Endoplasmic reticulum-associated degradation is required for nephrin maturation and kidney glomerular filtration function

Sei Yoshida[1,2,10] *, Xiaoqiong Wei[1,10], Gensheng Zhang[1,10], Christopher L. O'Connor[3], Mauricio Torres[1], Zhangsen Zhou[1], Liangguang Lin[1], Rajasree Menon[3], Xiaoxi Xu[4], Wenyue Zheng[2], Yi Xiong[5], Edgar Otto[3], Chih-Hang Anthony Tang[6], Rui Hua[2], Rakesh Verma[3], Hiroyuki Mori[1], Yang Zhang[7], Chih-Chi Andrew Hu[6], Ming Liu[4], Puneet Garg[3], Jeffrey B. Hodgin[8], Shengyi Sun[5], Markus Bitzer[3], Ling Qi[1,9] *

[1] Department of Molecular & Integrative Physiology, University of Michigan Medical School, Ann Arbor, MI 48105, USA

[2] State Key Laboratory of Medical Chemical Biology, College of Life Sciences, Frontiers Science Center for Cell Responses, Nankai University, Tianjin, 300071, China

[3] Division of Nephrology, Department of Internal Medicine, University of Michigan Medical School, Ann Arbor, MI 48105, USA

[4] Department of Endocrinology and Metabolism, Tianjin Medical University General Hospital, Tianjin, 300052, China

[5] Center for Molecular Medicine and Genetics, Department of Biochemistry, Microbiology and Immunology, Wayne State University, Detroit, MI 48201, USA

[6] Houston Methodist Cancer Center, Houston Methodist Academic Institute, Houston, TX 77030, USA

[7] Departments of Computational Medicine and Bioinformatics and Biochemistry, University of Michigan, Ann Arbor, MI 48109, USA

[8] Department of Pathology, University of Michigan Medical School, Ann Arbor, MI 48105, USA

[9] Division of Metabolism, Endocrinology & Diabetes, Department of Internal Medicine, University of Michigan Medical School, Ann Arbor, MI 48105, USA

[10] These authors contribute equally

*** Correspondence:** Ling Qi, University of Michigan Medical School, 5325 Brehm Tower, 1000 Wall St., Ann Arbor, MI 48105. Phone: (734) 936-4720. Email: lingq@med.umich.edu; Sei Yoshida, Nankai University College of Life Sciences, 94 Weijin Road, Tianjin, China 300071. Email: seiyoshi@nankai.edu.cn.

Running title: The key role of podocyte ERAD in health and disease

Keywords: Sel1L-Hrd1 ERAD, nephrin, disease mutants, ER, foot process, slit diaphragm

Summary: Mice with Sel1L deficiency in podocytes exhibit congenital nephrotic syndrome, at least in part, due to the impaired maturation of nascent nephrin in the ER.

The authors have declared that no conflict of interest exists.

None of our funding agencies requires a Creative Commons CC-BY license in order to support publication fees for this manuscript.

ABSTRACT

Podocytes are key to kidney glomerular filtration barrier by forming slit diaphragm between interdigitating foot processes; however, molecular details and functional importance of protein folding and degradation in the ER remain unknown. Here we show that SEL1L-HRD1 protein complex of endoplasmic reticulum (ER)-associated degradation (ERAD) is required for slit diaphragm formation and glomerular filtration function. SEL1L-HRD1 ERAD is highly expressed in podocytes of both mouse and human kidneys. Mice with podocyte-specific *Sel1L* deficiency develop podocytopathy and severe congenital nephrotic syndrome shortly after weaning with impaired slit diaphragm, and die prematurely with a median life span of ~3 months. Mechanistically, we show that nephrin, a type-1 membrane protein causally linked to congenital nephrotic syndrome, is an endogenous ERAD substrate. ERAD deficiency attenuates the maturation of nascent nephrin, leading to its retention in the ER. Lastly, we show that various autosomal-recessive nephrin disease mutants are highly unstable and degraded by Sel1L-Hrd1 ERAD, which attenuates the pathogenicity of the mutants towards the wildtype allele. Hence, this study uncovers a critical role of Sel1L-Hrd1 ERAD in glomerular filtration barrier function and provides new insights into the pathogenesis associated with autosomal recessive disease mutants.

INTRODUCTION

The key function of the kidneys is the ultrafiltration of blood in the glomerulus where podocytes, specialized differentiated epithelial cells, wrap around capillaries of the glomerulus via a unique cellular structure called foot process (1). The interaction between interdigitating foot processes is connected by the specialized cell junction known as the slit diaphragm, forming the filtration barrier. The slit diaphragm is composed of multi-protein complexes including membrane proteins nephrin and podocin, as well as cytosolic adapter protein CD2-associated protein (CD2AP), adhesion protein zonula occludens-1 (ZO1), and actin-associated protein synaptopodin (2-4). Loss of function of any of these factors in mice and humans leads to podocyte injury (i.e. podocytopathy) and renal failure due to impaired foot process function and the disruption of slit diaphragm (3-8).

Congenital nephrotic syndrome of the Finnish type (*NPHS1*, MIM 256300) is an autosomal recessive disease where the nephrin gene is mutated (3, 7), and is characterized by massive proteinuria, lack of slit diaphragm and foot processes, and premature death before 3 months of age in humans if left untreated (9-12). In mice, loss of nephrin leads to death within 24 hr after birth (8, 13). Nephrin is a type-1 transmembrane protein belonging to the immunoglobulin (Ig) superfamily with 10 glycosylation sites and eight disulfide bonds (14). However, molecular events underlying the biogenesis of nascent nephrin proteins as well as the role and significance of ER quality-control machineries in this process remain largely unexplored. Pointing to the significance of these questions, several of the over 250 nephrin mutations, mostly autosomal recessive in humans, have been shown to be retained in the endoplasmic reticulum (ER) (14, 15).

ER homeostasis has been proposed to be important for podocyte function and the development of kidney diseases, although the precise mechanism remains unknown (16-18). ER homeostasis is maintained mainly by three principal quality-control machineries, namely ER-associated degradation (ERAD), the unfolded protein response (UPR), and macroautophagy (hereafter, “autophagy”). Activation of the mTORC1 pathway evokes ER stress, resulting in podocyte loss and the development of nephrotic syndrome in podocyte-specific *Tsc1*-deficient mice at 3-4 weeks of age (19, 20). In addition, overexpression of pathogenic mutations of Laminin β 2 (*Lamb2),* α actinin-4 *(Actn4),* or collagen IV *(Col4a3)* activates UPR in podocytes (11, 21-23). In the case of *Lamb2* mutation at Cysteine residue 321 to Arginine (C321R) causes podocyte cell injury and/or nephrotic syndrome in transgenic mouse models (11, 21). However,

deletion of the IRE1α-XBP1 pathway of the UPR (either *Ire1a* or *Xbp1)* or *Atg5* of autophagy in podocytes has little-to-no impact on foot process and renal function during the first year of life in mice, and only caused mild albuminuria after 1 year of age (24-26). These data suggest that IRE1α of UPR and autophagy are largely dispensable for podocyte development and function in adult mice under basal condition.

These findings beg an important question of how ER homeostasis is maintained in podocytes, if the IRE1α-XBP1 pathway or autophagy is dispensable. ERAD is the principal quality control mechanism responsible for the recruitment and retrotranslocation of (misfolded) ER-resident proteins for proteasomal degradation (27-29). The Sel1L-Hrd1 complex represents the most conserved ERAD branch, with Sel1L being an obligatory cofactor for the E3 ligase Hrd1 (30-33). Recent studies have provided compelling evidence for the pathophysiological significance of Sel1L-Hrd1 ERAD in many cell types including hepatocytes, neuroendocrine, adipocytes, immune, intestinal epithelial, pancreatic acinar and β cells (27, 34-49). Indeed, Sel1L-Hrd1 ERAD plays a key role in normal physiology such as food intake, water homeostasis and energy metabolism in a substrate-specific manner (27, 28, 34). In many of these cellular systems, cells seem able to adapt to Sel1L-Hrd1 ERAD deficiency and, the effect of Sel1L-Hrd1 ERAD deficiency on cellular function may be uncoupled from ER stress or cell death, presumably (in part) due to the adaptive upregulation of ER chaperones, compensatory activation of other ERAD machineries, and/or protein aggregation that attenuates proteotoxicity of misfolded proteins (27, 28).

Here we report a key role for Sel1L-Hrd1 ERAD in podocytes in the pathogenesis of podocytopathy and congenital nephrotic syndrome. Indeed, unlike *Ire1a*-deficient mice, mice with podocyte-specific *Sel1L* deficiency develop podocytopathy and severe congenital nephrotic syndrome shortly after weaning. It does so, at least in part, by degrading misfolded nascent nephrin protein in the ER, which represents a key regulatory step in the formation of slit diaphragm.

RESULTS

SEL1L-HRD1 is expressed in human podocytes

We first determined gene expression pattern of SEL1L-HRD1 ERAD in kidneys using single cell RNA sequencing (scRNA-seq) analysis. A total of 2,545 cells collected from a human normal kidney sample (50, 51) were analyzed and led to the identification of 16 cell populations, of which only ~1-2% of total cells represented podocytes (Figure S1A). Both *SEL1L* and *HRD1* mRNA were ubiquitously detected in many cell types including podocytes and tubular cells, so were UPR sensor *IRE1α* (encoded by *ERN1*) and ER chaperone *BiP* (encoded by *HSPA5*) (Figure S1B-E). Similar observations were made upon the analysis of previously published scRNA-seq data of 24 human kidneys (52) (not shown).

To detect SEL1L protein level in kidneys, we generated a SEL1L antibody using a recombinant human SEL1L fragment (amino acids 23 to 194) (43). In glomeruli of healthy kidneys, SEL1L protein was detected in podocytes that were identified using the podocyte marker nuclear Wilms' tumor 1 (WT1) proteins (asterisks, Figure 1A). In addition, SEL1L was also detected in distal tubular cells (arrowheads, Figure 1A), although this still needed to be confirmed using cell type-specific markers. Similar expression pattern in the kidneys was observed for HRD1 (Figure 1B). As HRD1 stability and function depend on SEL1L (35, 53, 54), we concluded that the SEL1L-HRD1 ERAD complex is expressed in podocytes of human kidneys.

SEL1L-HRD1 expression in podocytes of patients with nephrotic syndrome

FSGS represents a common form of nephrotic syndrome, with initial podocyte injury followed by foot process effacement, and can be caused by a variety conditions (55). We next tested whether SEL1L-HRD1 expression is altered in podocytes of three patients with FSGS, with two "healthy" donor samples as controls. It is important to note that demographic information (e.g. age, race, gender and etc), the cause and severity of the disease, and medications were unknown to the researchers. We randomly grouped them into two experimental groups, healthy1-FSGS1 and health2-FSGS2-FSGS3. Each group was prepared at the same time and imaged under the same settings. In one patient (FSGS-1), SEL1L and HRD1 protein levels in podocytes were significantly decreased when compared to those in healthy individual (Healthy1) (Figure S2A-B and quantitated in Figure S2C-D). By contrast, in two other patients (FSGS-2 and 3), SEL1L protein level seemed to be elevated compared to those in another healthy individual (Healthy2), while HRD1 protein level was unchanged, compared to that of another healthy individual (Healthy2) (Figure S2A-B and quantitated in Figure S2C-D). While a much larger sample size would be needed to conclude how the expression of ERAD in podocytes changes

with disease initiation and progression, these observations suggested a possible role of SEL1L-HRD1 ERAD in podocytes.

Premature lethality of *Sel1L*^{PodCre} mice at ~3 months of age

In mouse glomeruli, Sel1L and Hrd1 proteins were also expressed in WT1+ podocytes (asterisks, Figure 2A-B). To explore the importance of Sel1L-Hrd1 ERAD in podocytes, we generated podocyte-specific Sel1L-deficient mice (*Sel1L*^{PodCre}) by crossing *Sel1L* floxed (*Sel1L*$^{f/f}$) mice (35) with Cre recombinase transgenic mice under the control of a highly podocyte-specific promoter *Podocin* (which becomes active during nephrogenesis in newborn kidneys) (56). Wildtype *Sel1L*$^{f/f}$ and heterozygous *Sel1L*$^{PodCre/+}$ littermates were included as controls. To assess the relative importance of ERAD vs. IRE1α in podocytes, we generated podocyte-cell specific *Ire1a*-deficient mice (*Ire1a*^{PodCre}) and performed a side-by-side comparison with age- and gender-matched *Sel1L*^{PodCre} mice.

Sel1L was specifically deleted in WT1-positive podocytes as demonstrated using immunofluorescent co-labeling of Sel1L and WT1 (asterisks, Figure 2A). In keeping with the notion that Sel1L is required for Hrd1 protein stability (35), Sel1L deletion also led to the reduced Hrd1 protein level in podocytes (asterisks, Figure 2B). Quantitation of Sel1L and Hrd1 protein levels in podocytes is shown in Figure 2C. For the first several weeks post-weaning, *Sel1L*^{PodCre} mice of both genders appeared largely normal when compared to their wildtype *Sel1L*$^{f/f}$ littermates (Figure 2D). However, starting from 6 weeks of age, *Sel1L*^{PodCre} mice began to lose body weight as they were getting sick (Figure 2D). *Sel1L*^{PodCre} mice had a median lifespan of ~13 weeks, with 14 and 10 weeks for males and females, respectively (Figure 2E-G). By contrast, *Ire1a*^{PodCre} mice appeared normal in terms of growth and life span compared to wildtype littermates within the first 6 months of life (blue, Figure 2D-G), suggesting that IRE1α of UPR is dispensable for podocyte function during this time period. For clarity, only the 10-week time point is shown for *Ire1a*^{PodCre} mice in Figure 2D. Moreover, heterozygous *Sel1L*$^{PodCre/+}$ littermates appeared normal, suggesting that in podocytes one copy of Sel1L is sufficient for ERAD function (gray, Figure 2D-G). Hence, we concluded that podocyte-specific Sel1L-deficient mice exhibit premature death with a median lifespan of ~13 weeks.

Congenital nephrotic syndrome and renal failure of *Sel1L*^{PodCre} mice

We next addressed how podocyte-specific deletion of Sel1L leads to early lethality in mice. At 3-5 weeks of age, *Sel1L*^{PodCre} kidneys appeared normal in color, but became pale at 10 weeks of

age (Figure 3A). Starting at 5 weeks of age, *Sel1L*^{PodCre} mice exhibited proteinuria, as demonstrated by the presence of albumin in the urine (Figure S3A and quantitated in Figure S3B). The ratio of albumin to creatinine in the urine of *Sel1L*^{PodCre} mice was elevated starting at 5 weeks of age when compared to wildtype littermates (Figure 3B). Similarly, blood concentrations of creatinine, cholesterol, and blood urea nitrogen (BUN), indicators of kidney function, were elevated starting at 7 weeks of age in *Sel1L*^{PodCre} mice (Figure 3C-D and S3C). On the other hand, the level of serum alanine aminotransferase (ALT), an indicator of liver function, was unchanged with age, even at 10 weeks of age when many *Sel1L*^{PodCre} mice were moribund (Figure S3D), excluding the possible contribution from secondary liver damage in disease pathogenesis. By contrast, 10-week-old *Ire1a*^{PodCre} mice appeared normal in terms of proteinuria, serum levels of creatinine, cholesterol, and BUN (Figure S3B-C, S3E and 3C-D).

Histochemical examination of the kidneys from 3-week-old cohorts revealed normal morphology of the kidney medulla, cortex and glomeruli (Figure 3E-G). However, at 5 weeks of age, renal tubules in both the cortex and medulla were filled with large protein casts in *Sel1L*^{PodCre} mice (asterisks, panel 5 vs. 6 and 7 vs. 8, Figure 3H-I). Moreover, although the size of glomeruli was similar between the cohorts, *Sel1L*^{PodCre} glomeruli exhibited mesangial cell hyperplasia (marked with #) with reduced open capillary loops (yellow arrowheads, panel 9-10, Figure 3J). Quantitation of glomeruli size and mesangial cell hyperplasia are shown in Figure S3F-G. Unlike flattened podocytes at the peripheral of glomeruli in wildtype mice, *Sel1L*^{PodCre} podocytes were rounded (black arrows, panel 9-10, Figure 3J). Taken together, we concluded that disease initiation in *Sel1L*^{PodCre} mice occurs around 3-5 weeks of age, and that Sel1L deficiency in podocytes leads to early-onset renal failure and premature death.

Impaired slit diaphragm in *Sel1L*^{PodCre} mice

We next performed scanning electron microscopy (SEM) to visualize glomeruli and podocytes from 3-, 5- and 10-week-old mice. Images from two independent samples are shown for each age in Figure 4A-C and S4A-C. At 3 weeks of age, glomeruli appeared largely normal in size, shape and overall morphology in *Sel1L*^{PodCre} mice (Figure 4A, S4A). Podocytes formed primary and secondary processes (PP and SP), as well as interdigitating foot processes (FP) in *Sel1L*^{PodCre} mice. However, starting at 5 weeks of age, *Sel1L*^{PodCre} mice exhibited broadened PP and shortened SP (Figure 4B, S4B). Moreover, interdigitating FP between podocytes were dramatically disorganized and misdirected, similar to those in nephrin-deficient mice (8, 57, 58). The defects in foot processes became more severe with age in *Sel1L*^{PodCre} mice: by 10 weeks of

age, some glomeruli were severely damaged and showed foot process effacement (Figure 4C, S4C).

We next performed transmission electron microscopy (TEM) to visualize ultrastructural changes of podocytes and the filtration unit at different ages. In healthy glomeruli, three layers, the innermost endothelium (ENDO), the glomerular basement membrane (GBM), and the podocytes with interdigitating foot processes (FP), form the glomerular filtration barrier of the kidneys (1). At 3 weeks of age, three layers of the filtration unit appeared largely normal (Figure 4D and Figure S4D). However, at 5 weeks, *Sel1L*^{PodCre} mice exhibited mesangial cell hyperplasia (asterisks) and fusion of foot processes (black arrows, Figure 4E, S4E).

Interdigitating foot processes are held together by an extracellular structure known as the slit diaphragm (arrows, Figure 4F and diagram shown in Figure 4G) (2, 3). Quantitation of the length of slit diaphragm showed its length being around 40 nm in 5-week-old wildtype mice (Figure S4F), consistent with previous reports (57, 59-61). On the other hand, *Sel1L*^{PodCre} podocytes had very few slit diaphragm: the junctions between the remaining adjacent foot processes were very narrow (arrow, Figure 4F). This was further confirmed using ultra-high resolution advanced SEM analyses, in comparison with regular SEM on the same podocytes (Figure S5A), where slit diaphragm was visible as a bridge-like structure linking adjacent foot processes in wildtype mice, but largely absent in *Sel1L*^{PodCre} mice at 5 weeks of age (red arrows, Figure 4H, S5B-C). Hence, we concluded that Sel1L deficiency in podocytes leads to impaired slit diaphragm at 5 weeks of age, which coincides with the development of proteinuria and nephrotic syndrome.

Maturation defect of nephrin protein in *Sel1L*^{PodCre} mice *in vivo*

Nephrin, together with other proteins such as the ER protein podocin, and cytosolic proteins CD2AP and synaptopodin, forms slit diaphragm (Figure 4G). We next explored whether and how Sel1L deficiency in podocytes affects the intracellular localization of these proteins by performing co-staining with markers for the ER (KDEL) and slit diaphragm (ZO1). In wildtype podocytes, nephrin exhibited a diffused pattern surrounding the nucleus (Figure 5A), and with some colocalization with KDEL after artificial saturation of KDEL signal (arrows, S6A). In addition, nephrin was distributed basally adjacent to the GBM along the peripheral capillary loops, as demonstrated by its colocalization with cell junction protein ZO1 (arrows, Figure 5B). ZO1 continuously distributes along GBM as shown previously (62, 63). By contrast, in

Sel1L^{PodCre} podocytes, the colocalization between nephrin and the ER maker KDEL was significantly increased (Figure 5A), while the colocalization between nephrin and ZO1 were significantly decreased (Figure 5B). Of note, KDEL level was increased in the absence of Sel1L likely as a result of cellular adaptive response to ERAD deficiency (37, 38).

In direct contrast to nephrin, maturation of another key component of silt diaphragms, podocin (encoded by *NPHS2*), in the ER seemed unaffected in *Sel1L*^{PodCre} podocytes as they were able to exit the ER (i.e. lack of colocalization with KDEL, Figure 5C) and, for some, reached to the GBM along the peripheral capillary loops (i.e. colocalization with ZO1, arrows, Figure 5D). Moreover, distribution of actin-associated primary process markers, CD2AP (arrows, Figure 5E) and synaptopodin (arrows, Figure S6B) along GBM was unaffected by *Sel1L* deficiency.

To further demonstrate biochemically how nephrin maturation is affected by Sel1L-Hrd1 ERAD, we next performed various biochemical assays. It is well documented that nephrin proteins appeared as two bands on SDS-PAGE around 180 kDa, slow-migrating mature a (nephrin *a*) and fast-migrating ER-retained b forms (nephrin *b*), as a result of differential glycosylation at ten potential *N*-glycosylation sites (15, 64-66). In wildtype mice, the percent of nephrin *b* in total nephrin was about 50% at 3 weeks of age, and decreased with age, reaching 35 and 25% at 5 and 7 weeks of age, respectively (Figure 5F and quantitated in Figure 5G). By contrast, in *Sel1L*^{PodCre} kidneys, the percent of nephrin *b* was mildly elevated about 60% at 3 weeks of age, but significantly increased with age, reaching 70 and 85% at 5 and 7 weeks of age, respectively (Figure 5F and quantitated in Figure 5G). Of note, at 7 weeks of age, total nephrin protein level was significantly decreased in *Sel1L*^{PodCre} kidneys (Figure 5F), likely resulted from elevated podocyte loss as observed in SEM (Figure S4C). Furthermore, in the purified microsomal fractions (containing the ER and other endomembranes) from kidneys of 3-week-old mice, total amount and percent of ER-retained b form nephrin was elevated in *Sel1L*^{PodCre} kidneys (Figure S6C), providing further support for elevated ER accumulation of nephrin in *Sel1L*^{PodCre} podocytes as revealed in immunofluorescence staining (Figure 5A).

We next subjected kidney lysates to endoglycosidase H (EndoH) digestion to distinguish immature high-mannose EndoH sensitive forms (i.e. present in the ER) from those EndoH resistant forms (i.e. mature beyond the ER). The EndoH sensitive fraction of total nephrin protein was about 40% in wildtype vs. 60% in *Sel1L*^{PodCre} kidneys at 5 weeks of age (Figure 5H and quantitated in Figure S6D). As controls, podocin, which has no predicted glycosylation

sites, as well as cytosolic protein synaptopodin, were largely unchanged in *Sel1L*^{PodCre} kidneys at different ages (Figure 5H, S6E). Taken together, we concluded that Sel1L deficiency causes defects in the maturation of nephrin in the ER, while having no notable effect on the localization and protein levels of other major slit diaphragm proteins such as CD2AP, podocin and synaptopodin.

Normal nephrin maturation in *Ire1α*-deficient podocytes

We next asked whether nephrin defect is specific for Sel1L deficiency. To this end, we analyzed the status of nephrin protein in *Ire1a*^{PodCre} mice (Figure S7). The ratio of *b*- to *a*-forms of nephrin was comparable between *Ire1a*^{PodCre} mice and their wildtype littermates from 3 to 7 weeks of age (Figure S7A, and quantitated in Figure 5G). Similarly, podocin and synaptopodin levels were comparable between the cohorts at different ages (Figure S7B). Moreover, confocal microscopy revealed that, in *Ire1a*^{PodCre} podocytes, nephrin protein was present surrounding the nucleus and basally adjacent to the GBM along the peripheral capillary loops, similar to those in wildtype littermates (arrows, Figure S7C). Hence, the defects of nephrin in *Sel1L*^{PodCre} mice are uncoupled from IRE1α of UPR.

Maturation defect of nascent nephrin protein in *ERAD*-deficient cells *in vitro*

To further demonstrate the impact of *Sel1L* deficiency on nephrin folding, we performed immunoprecipitation of nephrin in 5-week-old kidneys. There was elevated interaction between nephrin and BiP, a key ER chaperone involved in protein folding and degradation, in *Sel1L*^{PodCre} kidneys (Figure 6A). This finding provided a plausible explanation for the delayed maturation and ER accumulation of nephrin in *Sel1L*-deficient cells and pointed to the effort to (re-)fold nephrin in the absence of ERAD. Hence, we speculated that nephrin may be misfolding prone and subjected to quality control by Sel1L-Hrd1 ERAD.

To further establish the causal relationship between Sel1L deficiency and nephrin maturation, we performed the following experiments *in vitro*. We first generated *HRD1*-deficient human podocytes using the CRISPR/Cas9 system (Figure 6B). In line with other cell types (37, 38, 43), HRD1 deletion in podocytes stabilized Sel1L protein, leading to its accumulation (Figure 6B). In *HRD1*-deficient human podocytes, nephrin accumulated and was predominantly retained in the ER, similar to *Sel1L*^{PodCre} podocytes (Figure 6C). Next, we generated *HRD1*-deficient human embryonic kidney HEK293T cell line, which do not express endogenous nephrin. Similar to endogenous nephrin in kidneys, loss of HRD1 increased the proportion of nephrin *b* (lane 1 vs.

4) as well as EndoH sensitive form of nephrin (51 % vs. 5% in WT) (lane 3 vs. 6, Figure 6D). Overexpressing of HRD1 in *HRD1*-deficient HEK293T cells reversed nephrin maturation defects and increased the percent of nephrin *a* (Figure S8A). Differential mobility shift in EndoH-treated samples was due to glycosylation as the EndoH resistant form was sensitive to PNGase F treatment, which removes almost all *N*-linked oligosaccharides from glycoproteins (lane 2 vs. 5, Figure 6D).

Third, to directly visualize nascent protein maturation in the ER, we performed ^{35}S metabolic labeling followed by chase for different time points in Myc-tagged nephrin-transfected HEK293T cells. Strikingly, nearly 50% nascent nephrin proteins matured to nephrin *a* within 4 hr in wildtype cells vs. only 20% in *HRD1*$^{-/-}$ cells (Figure 6E and quantitated in Figure 6F). Taken together, these data suggested that Sel1L-Hrd1 ERAD is required for the maturation of nascent nephrin protein in the ER.

Nephrin is a *bona fide* endogenous ERAD substrate

Decreased nephrin maturation and elevated association with BiP in ERAD-deficient cells prompted the hypothesis that nephrin is an endogenous ERAD substrate. We first asked whether nephrin is ubiquitinated by Sel1L-Hrd1 ERAD. In a gain-of-function assay, HEK293T cells were transfected with nephrin, together with Myc-tagged wildtype Hrd1 or E3 ligase-dead C2A Hrd1 mutant. Indeed, nephrin interacted with Hrd1 and was ubiquitinated by Hrd1 in an E3-ligase dependent manner (lane 4 vs. 6, Figure S8B). Conversely, in the absence of HRD1, ubiquitination of nephrin was significantly reduced compared to wildtype cells (lane 4 vs. 5, Figure 6G). Ubiquitination of nephrin was only seen in cells treated with the proteasomal inhibitor MG132 (lane 2-3 vs. 4-5, Figure 6G), pointing to the involvement of proteasome in this process. Moreover, in line with the *in vivo* data (Figure 6A), nephrin interacted strongly with BiP in *HRD1*$^{-/-}$ HEK293T cells (lane 2 vs. 3, Figure 6G). Next, we determined the half-life of nephrin in transfected HEK293T cells treated with the translation inhibitor cycloheximide (CHX). Cells were pretreated with brefeldin A (BFA) to block ER exit and as a result, nephrin was predominantly in the *b* form (Figure 6H). Nephrin in wildtype cells quickly decreased with a half-life of 2 hr; however, that process was significantly delayed in *HRD1*$^{-/-}$ cells, with a half-life beyond 4 hr (Figure 6H).

What is the significance of ERAD-mediated degradation of misfolded wildtype nephrin? To this end, we tested whether ERAD attenuates the aggregation of misfolded nephrin proteins.

Indeed, the abundance of nephrin-containing high molecular weight (HMW) complexes with a molecular weight of over 250 kDa was increased by approximately 1.4-folds in transfected *Hrd1*$^{-/-}$ cells compared to that in wildtype cells (Figure 6I). These HMW complexes were formed via disulfide bonds as they were sensitive to the treatment of a reducing agent β-mercaptoethanol (Figure 6I). Taken together, we concluded that nephrin is a bona fide substrate of Sel1L-Hrd1 ERAD and that ERAD of misfolded nephrin is required for its maturation in the ER.

Pathogenic nephrin mutants are SEL1L-HRD1 ERAD substrates

To further establish the pathological importance of SEL1L-HRD1 ERAD, we explored its role in the maturation of pathogenic nephrin mutants (Figure 7A). Nephrin was predicted to consist of 8-9 extracellular Ig domains, followed by a fibronectin (FN) type III-domain, a transmembrane (TM) region, and a cytosolic tail (3, 7). We first performed structural modeling analysis of nephrin using a recently developed program, C-I-TASSER (67), which predicted that, in addition to the FN and TM domains, nephrin protein consists of 9 Ig domains (Figure 7A).

Among many nephrin mutants identified in humans with congenital nephrotic syndrome, a subset of mutants is known to cause, to a certain extent, ER retention (15, 64, 65). We randomly picked six nephrin missense mutations, I171N, G270C, S366R, S724C, R743C, and L832P located at different Ig domains for further analyses (Figure 7A). C-I-TASSER analysis of each mutant revealed how each mutation changed local conformation and the interaction with nearby residues (Figure 7B-C and S9A-D). For example, the I171N mutation would alter the formation of a hydrophobic core consisted of I171, P169 and V198, whereas the G270C mutation would lead to the formation of a C270-C265 disulfide bond and abolish the C317-C265 disulfide bond (Figure 7B-C). Next, we measured the impact of each mutation on the protein folding in terms of ΔΔG, i.e. the free energy change caused by a single mutation, using EvoEF2 (68), a newly developed empirical force field for protein design and mutation effect analysis. ΔΔG of these mutants ranged from + 37.8 (S724C) to +230.9 (S366R) versus 0 (wildtype) (in blue, Figure 7A). A higher ΔΔG indicates less stability, suggesting that these mutants are likely unstable.

Unlike wildtype nephrin, all six mutants appeared on SDS-PAGE predominantly (over 80-100%) as the fast-migrating *b* form in both WT and *HRD1*$^{-/-}$ HEK293T cells (Figure 7D and quantitated in Figure 7E). Consistently, EndoH digestion revealed that these six nephrin mutants were EndoH sensitive, i.e. retained in the ER (Figure 7F and S9E), which was confirmed using

confocal microscopy for G270C (Figure S9F). Furthermore, all mutants were degraded by SEL1L-HRD1 ERAD as they were stabilized in *HRD1*$^{-/-}$ HEK293T cells treated with CHX for 4 hr (Figure 7G and quantitated in Figure 7H). Hence, these data showed that all 6 human mutants are retained in the ER where they are degraded by SEL1L-HRD1 ERAD.

ERAD of mutant nephrin reduces its aggregation propensity and pathogenicity

Lastly, we explored the pathological significance of ERAD-mediated degradation of human mutants. ERAD deficiency triggered most nephrin mutants (with the exception of S366R) to form HMW complexes (Figure 8A-B), and the effect was much more dramatic than that towards the wildtype nephrin (vs. lanes 1-2, Figure 8A). These mutants also formed more detergent (0.5% NP40)-insoluble protein aggregates in ERAD-deficient cells (Figure 8C). Hence, these data showed that SEL1L-HRD1 ERAD mediates the degradation of nephrin mutants, thereby attenuating their aggregation.

While these mutants are aggregation prone, one allele is insufficient to cause disease (i.e., autosomal recessive). Hence, we asked whether ERAD attenuates the pathogenic effect of mutants towards the wildtype allele. Wildtype nephin was tagged with the Myc tag, while the mutants (I171N and G270C) were either untagged or tagged with Flag – thereby to distinguish the two forms. In wildtype HEK293T cells, co-expression of mutant nephrin had little/no effect (10-20% increase) on the HMW formation of wildtype nephrin compared to wildtype nephrin alone (lane 5-6 vs. 2, Figure 8D). However, in *HRD1*$^{-/-}$ cells, co-expression of mutant nephrin significantly enhanced by 2.5-3 folds the HMW complex formation of wildtype nephrin compared to wildtype nephrin alone (lane 10-11 vs. 7, Figure 8D). Moreover, co-expression of mutant nephrin reduced the total wildtype nephrin protein level in wildtype cells in a dose-dependent manner, while having no effect on the maturation efficiency as quantitated by the percent of nephrin *a* in total nephrin (lane 2 vs. 3-4 and 5-6, Figure 8E and quantitated in Figure 8F). By contrast, co-expression of mutant nephrin in *HRD1*$^{-/-}$ cells did not affect total wildtype nephrin levels, but reduced the percent of nephrin *a* form in a dose-dependent manner (lane 8 vs. 9-10 and 11-12, Figure 8E and quantitated in Figure 8F). These data suggested that, while mutant nephrin promotes the degradation of wildtype nephrin in ERAD-competent cells, it only interferes with the maturation of wildtype nephrin in ERAD-deficient cells, not in ERAD-competent cells. Hence, we concluded that SEL1L-HRD1 ERAD degrades nephrin mutants, thereby ensuring normal maturation of wildtype allele.

DISCUSSION

Here our data demonstrate that SEL1L-HRD1 ERAD in podocytes plays a critical role in the formation of slit diaphragm and glomerular filtration function. Sel1L deficiency in podocytes impairs slit diaphragm integrity and leads to podocytopathy, congenital nephrotic syndrome and renal failure, starting at 3-5 weeks after birth. Our side-by-side comparison with mice carrying podocyte-specific deletion of UPR sensor IRE1α show that IRE1α is dispensable for podocyte function at the same age, in keeping with the conclusions from previous studies (24, 25). Together with recent studies (27, 28, 34, 69), these findings unequivocally establish a vital importance of Sel1L-Hrd1 ERAD in podocyte function.

Our data further suggest that ERAD effect in podocytes is largely substrate-dependent. Nascent nephrin protein is misfolding prone and ubiquitinated by SEL1L-HRD1 ERAD for proteasomal degradation. In the absence of ERAD, misfolded nephrin accumulates in the ER and may undergo further refolding or interfere with the normal maturation process for nascent nephrin protein. Indeed, our data show that interaction between nephrin and BiP is enhanced in the absence of ERAD, and so are the nephrin-containing HMW protein complexes. Moreover, the proportion of ER-retained nephrin *b* form is progressively increased in *Sel1L*^{PodCre} kidneys starting at 3 weeks of age, in direct contrast to those in wildtype kidneys where mature nephrin *a* form is elevated with age. Hence, we conclude that SEL1L-HRD1 ERAD plays an indispensable role in podocyte function, at least in part, by regulating the maturation of nascent nephrin protein in the ER. While it has been reported that intracellular distribution of nephrin is altered in humans with FSGS (70, 71), it remains unclear whether SEL1L-HRD1 ERAD plays a role in the disease pathogenesis. Our initial data showed that expression of SEL1L-HRD1 ERAD is altered in patients with FSGS; however, significantly larger sample size with consideration of patient age, gender, race, disease state, medications and the nature of the control samples, is required to address this question in the future.

While some nephrin mutations in humans with congenital nephrotic syndrome – mostly autosomal recessive – are known to be retained in the ER (14, 15), our understanding of the molecular events associated with the biogenesis of nascent nephrin proteins, especially in regards to their interactions with quality control machineries, remained largely unexplored. In this study, we report that SEL1L-HRD1 ERAD mediates the degradation of all 6 pathogenic

mutants, which may attenuate not only their accumulation and self-aggregation in the ER, but also their pathogenicity towards the wildtype allele. In the absence of ERAD, these nephrin mutants readily form HMW and insoluble aggregates, which include some wildtype nephrin protein. Indeed, the role of Sel1L-Hrd1 ERAD in podocytes bears resemblance to its role in the maturation of prohormones AVP and POMC in the pathogenesis of diabetes insipidus and obesity, respectively (37, 38). Hence, we speculate that enhancing SEL1L-HRD1 ERAD activity may reduce the dominant negative effects of mutant alleles in human diseases. How Sel1L-Hrd1 ERAD can identify and target misfolded nephrin remains unclear.

Cells constantly live under various physiological and pathological stresses. This is especially true for podocytes, which are responsible for maintaining the filtration barrier and face not only mechanical but also cellular stresses (including ER and oxidative stresses) and immunological challenges. These cells hence have a high capacity to preserve function by synthesis of glomerular basement membrane components, formation of the slit diaphragm, and enhancing endothelial cell survival (1). ER homeostasis is maintained mainly by three principal quality-control machineries, namely ERAD, UPR, and autophagy. The observation that deletion of *Ire1a-Xbp1* or *Atg5* has minimal effect on podocyte function (24-26) (and this study) again supports the notion that podocytes are highly resilient and adaptive. Moreover, our findings highlight the fundamental importance of Sel1L-Hrd1 ERAD as the first line of defense against misfolded proteins in the ER, and in the case of podocytes, Sel1L-Hrd1 ERAD is essential for slit diaphragm formation. It's worth pointing out that, at 7-10 weeks of age, we did observe podocyte loss as revealed by SEM analysis of glomerulus and the reduction in total nephrin and synaptopodin protein levels. These finding suggested that podocytes may not be able to tolerate chronic Sel1L-Hrd1 ERAD deficiency. However, as disease has already been initiated at 3-5 weeks of age in *Sel1L*^{PodCre} mice where glomeruli and podocytes appear largely normal, we believe that podocyte Sel1L-Hrd1 ERAD controls disease initiation, not due to cell death, but rather in a substrate-specific manner.

This study focuses on the maturation of nephrin, because of its pathophysiological importance and more importantly, because of the similarity between the *Sel1L*- and *Nephrin*-deficient mouse models. However, as *nephrin*-deficient mice die within 24 hr after birth (8) vs. ~13 weeks for podocyte-specific *Sel1L*-deficient mice, we acknowledge that Sel1L-Hrd1 ERAD deficiency unlikely causes a complete loss of function of nephrin. This is consistent with the biochemical results showing that some nephrin still mature beyond the ER even at 5-7 weeks of age. In

addition, we speculate that ERAD in podocytes may regulate the maturation of other proteins in a manner similar to nephrin, such as those involved in the generation of secondary and tertiary foot processes, which may also contribute to the early lethality of *Sel1L*^{PodCre} mice. While all these possibilities require further investigation, our findings demonstrate a crucial role of Sel1L-Hrd1 ERAD in podocyte function in health and disease.

METHODS AND MATERIALS

A. Human studies

Human tissue samples and immunofluorescence staining

De-identified formalin-fixed, paraffin embedded kidney sections (3 μm) from patients who were found to have FSGS on kidney biopsy (FSGS1-3) and living kidney donors were obtained from Pathology Department and used for the immunostaining of SEL1L and HRD1. Antigen retrieval was performed in boiling 10 mM sodium citrate buffer (pH 6.0) for 15 min. Antibodies was diluted in 5% donkey serum, 0.3% Triton X-100 in PBS. Slides were placed in a humidified chamber at 4°C overnight with primary Ab. Next day, slides were incubated with secondary antibodies for 1 h at room temperature. Following three washes with TBST, slides were incubated anti-WT1-Alexa Fluor 647 for 1 h at room temperature. Following washes with TBST and distilled water, 10 μl pro-long Gold antifade mounting media with DAPI (Invitrogen P36931) was applied. Samples were imaged with identical parameters under the Nikon A1 Confocal Microscope at the University of Michigan Imaging Core.

Antibodies

Antibodies used in the IF of human samples: SEL1L (43) (home-made E12049, specific for both human and mouse, rabbit, 1:500); HRD1 (kindly provided by Dr. Richard Wojcikiewicz, SUNY Upstate Medical University, Syracuse, New York, USA; rabbit, 1:50 for immunostaining); and WT1-Alexa Fluor 647 (Abcam ab202639, 1:500).

ScRNA-seq of the human kidney

Human kidney tissue obtained from the unaffected, tumor distant site of a 43-year-old male patient undergoing nephrectomy (warm and cold ischemic time < 5 minutes). Experimental details were described in the Supplemental Methods. ScRNA-seq data have been deposited in

the NCBI with the accession number PRJNA700694 (https://www.ncbi.nlm.nih.gov/bioproject/700694).

B. Mouse studies

Mice

The *Sel1L*$^{f/f}$ mice (35) were crossed with mice expressing Cre transgene driven by the *Podocin* promoter (56) on the C57BL/6 background to generate podocyte-specific Sel1L-decficient (*Sel1L*^{PodCre}) mice. Their littermates, *Sel1L*$^{f/f}$ (WT) and heterozygous (*Sel1L*$^{PodCre/+}$), were included as control cohorts. *Ire1a*$^{f/f}$ mice (72) were used to generate *Ire1a*^{PodCre} mice using the same breeding scheme. All the mice were housed in an ambient temperature room with 12 h light cycle and fed a normal-chow diet (13% fat, 57% carbohydrate, and 30% protein, LabDiet 5LOD). Weekly measurements of body weight were performed at the same time of the day. Mice at the ages of 3, 5, 7, and 10 weeks, both genders, were used in the studies.

Tissue fixation

After mice were anesthetized, the kidneys were perfused with cold PBS for 2 min, then with cold fixation buffer A [4% paraformaldehyde (Electron Microscopy Sciences, 50-980-487) and 2.5% glutaraldehyde (Electron Microscopy Sciences, 16000) in Sorensen's buffer (Electron Microscopy Sciences,11600-05)] for electron microscopy (EM) and Hematoxylin & Eosin (H&E) staining, or buffer B (10 % Formalin in PBS) for immunofluorescence staining. The samples were sent to Research Histology and Immunohistochemistry Core at the University of Michigan Medical School for paraffin processing, embedding and H&E staining.

Immunofluorescence staining and confocal microscopy

The kidneys were fixed in fixation buffer (10 % Formalin in PBS) at 4^0C overnight, transferred to cold PBS and incubated at 4^0C overnight, then transferred to cold PBS with 20 % sucrose at 4^0C for another overnight. Then the samples were frozen in Tissue-Tek O.C.T. Compound (Electron Microscopy Sciences) and kept at -80^0C. The frozen sections were prepared by cutting at 5 µm by a cryostat (CM1950, Leica). Wildtype and knockout tissues from the same litter were prepared on the same slide under the same condition and kept at -80^0C. For the staining, the slides were washed in PBS at room temperature 3 times followed by blocking buffer (5% BSA, 0.1% Tween, TBS) for 30 min at room temperature. Primary antibody was diluted in the blocking buffer and applied for the tissue areas at 4^0C overnight. Next morning, slides were washed with TBST (0.1 % Tween in TBS) for 10 min 3 times, then secondary

antibody solution was applied to incubate for 2 hr at room temperature. Samples were washed with TBST for 10 min 3 times and briefly washed with water before the mounting (ProLong Gold antifade reagent with DAPI, Invitrogen). Tissues on the same slide were imaged using identical imaging parameters under the Nikon A1 Confocal Laser Microscope (Microscopy Core at the University of Michigan). Signal intensities as well as the distribution patterns were compared under the same conditions.

Antibodies

Hrd1, Sel1L and WT1 antibodies for immunostaining were described as above. Sel1L (Abcam ab78298; 1:1000 for western blot), Podocin (Sigma-Aldrich, P0372; 1:100 for immunostaining and ABclonal A17337; 1:3000 for western blot), Hrd1 (Proteintech 13473-1-AP; 1:3000 for western blot), Synaptopodin (Santa Cruz sc-515842; 1:100 for immunostaining and ABclonal A12049; 1:2000 for western blot), Nephrin (ABclonal A3048; 1:2000 for western blot, 1:100 for immunostaining), KDEL (Abcam ab12223; 1:200 for immunostaining), ZO1 (Thermo Fisher 33-9100; 1:100 for immunostaining), BiP (Abcam ab21685; 1:5000 for western blot, 1:200 for immunostaining), CD2AP (Proteintech 51046-1-AP; 1:300 for immunostaining), Ub (Santa Cruz sc-8017; 1: 1000 for western blot), Myc (Sigma C3956; 1:5000 for western blot), Flag (Sigma F-1804; 1:5000 for western blot), HSP90 (Santa Cruz sc-13119; 1:5000 for western blot), Histone H2A (Cell Signaling Technology #2578; 1:2000 for western blot). Secondary antibodies for western blot were goat anti-rabbit IgG-HRP (Bio-Rad #5196-2504; 1:5,000) and anti-mouse IgG-HRP (Bio-Rad #1706516; 1:5,000), and for immunostaining were Alexa Fluor anti-mouse-IgG Alexa Fluor 594 (115-585-044), anti-mouse-IgG Alexa Fluor 488 (715-545-150), anti-rabbit-IgG Alexa Fluor 594 (111-585-144), and anti-rabbit-IgG Alexa Fluor 488 (711-545-152), which were all purchased form Jackson ImmunoResearch Laboratories and used at 1:500-1,000.

Imaging data analysis

Signal intensity of Sel1L/Hrd1 per podocyte was measured using ImageJ, which was further analyzed using ggplot2 as described in Human studies section. Image J was used to quantitate the glomerulus size and the index of mesangial hyperplasia. For the index of mesangial hyperplasia, we measured H&E-stained positive area in each glomerulus was divided by the area of whole glomerulus.

Transmission electron microscopy (TEM) and (advanced) scanning EM (SEM)

EM samples are prepared using standard methods as described previously (19, 58). The samples were submitted to the University of Michigan Microscope and Image Analysis core facility (MIL) for washing and embedding according to standard procedures. Embedded samples were analyzed by the JEOL USA JEM-1400 Plus Electron Microscope for TEM and the AMRAY 1910 Field Emission Scanning Electron Microscope for SEM. For ultra-high-resolution advanced SEM, samples were examined under the Thermo Fisher Helios 650 Nanolab SEM at the Michigan Center for Materials Characterization.

C. In vitro studies

Cell lines

The HEK293T and N2a cells, obtained from ATCC, were cultured in DMEM (10017CV, Corning) containing 10% FBS and 1% penicillin-streptomycin. *HRD1*$^{-/-}$ HEK293T and N2a cells were generated as described previously (38, 49). To generate *HRD1*$^{-/-}$ podocytes, immortalized human podocytes CIHP-1 (73) were grown at 33 °C to 80 % confluence in RPMI1640 (Corning 10-040-CM) supplemented with Insulin-Transferrin-Selenium (Gibco 51500-056), 10% FBS and 1% penicillin-streptomycin, sub-cultured at 1:3, and then incubated at 37^{0}C for 14 days to induce differentiation. At day 10, cells were transduced with lentiviral CRISPR system targeting HRD1 as previously described (49). Guide sequences for HRD1: GGGACAAAGGCCTGGATGTAC as the guide 1; GGGCCAGCCTGGCGCTGACCG as the guide 2.

Plasmids

HA-Ub, Hrd1-WT-Myc, and Hrd1-C2A-Myc plasmids were described previously (49). Mouse nephrin and myc-nephrin plasmids were described previously (74), from which we generated Flag-tagged nephrin using PCR. Quick-change mutagenesis was used to generate nephrin point mutants using the mouse nephrin constructs (49). The following primers were used for mutagenesis: I171N (5′- aagccagcacctgacaacatcttcatccagggt -3′, 5′- accctggatgaagatgttgtcaggtgctggctt -3′), G270C (5′- tgcatagccagaggttgtaatccacctgcgacc -3′, 5′- ggtcgcaggtggattacaacctctggctatgca -3′), S366R (5′- tgccttaccaagtccagacgcccacgggtcctg-3′, 5′- caggacccgtgggcgtctggacttggtaaggca -3′), S724C (5′- ctacactgccagaactgcgagggcaccgccgag-3′, 5′- ctcggcggtgccctcgcagttctggcagtgtag -3′), R743C (5′- tatgctcccaccatctgtgccctgaaggaccct -3′, 5′- agggtccttcagggcacagatggtgggagcata-3′), and L832P (5′- agaggactggttcgtcctgttgtccgatttgcc -3′, 5′- ggcaaatcggacaacaggacgaaccagtcctct -3′).

In vitro drug treatment

For the treatment with cycloheximide (CHX), MG132, and brefeldin A (BFA), experiments were performed as described previously (37, 41, 48, 49). Briefly, transfected HEK293T cells pretreated with BFA (1 μg/ml) for 30 minutes, followed by CHX for 2 and 4 hr. 10 μM MG132 was added to the culture at the last 5 hr prior to the experiments.

^{35}S pulse-chase experiment

HEK293T cells were transfected with myc- or flag-nephrin constructs followed by pulse-chase experiment. HEK293T cells were pulse labeled with 100 μCi/ml [^{35}S]-cysteine and methionine at 37 ℃ for 30 minutes. Following 30 min pulse, cells were cultured in chase medium (regular media supplemented with 10 mM HEPES, 5 mM cysteine, 5 mM methionine) for the indicated times. Cells were then washed with ice-cold HBSS buffer (Gibco, Life Technologies), snap-frozen in liquid nitrogen and lysed in NP-40 lysis buffer (1% NP-40, 150 mM NaCl, 1 mM EDTA, 50 mM Tris-HCl pH 8.0) supplemented with 100X proteinase inhibitor cocktail (Sigma), 1 mM PMSF (Sigma), and 10 mM N-ethylmaleimide. Lysates were used in the immunoprecipitation as described above. Denaturing samples were prepared by adding 2X denaturing sample buffer into the immunoprecipitated beads followed by 10 min boiling at 95 ℃.

Statistical Analyses

All experiments were conducted at least twice or with at least two biological replicates. Results are expressed as the mean ± SEM. Comparisons between two and multiple groups were made by unpaired, two-tailed Student's t-test and one-way ANOVA followed by Tukey's multiple comparison test, respectively, unless otherwise specified. For survival analysis, the Kaplan-Meier method and the log-rank test were used. P values of < 0.05 were considered statistically significant.

Study Approval

Human study was approved by the Institutional Review Board of the University of Michigan (HUM00002468). All animal procedures were approved by and done in accordance with the IACUC at the University of Michigan Medical School (PRO00008989).

AUTHOR CONTRIBUTION

S.Y. initiated, designed and performed in vivo studies; X.W. designed and performed some in vitro experiments and structural analysis; G.Z. repeated many in vivo and in vitro experiments, and performed some in vitro experiments. Both scientific and intellectual contributions was used to decide the authorship order among co-first authors (S.Y., X.W. and G.Z.). C.O.C., R.M., E.O., J.B.H. and M.B. provided scRNA-Seq data and human kidney samples; M.T. assisted with and performed electron microscopic studies; L.L., Z.Z., X.X., and Y.X., performed some biochemical assays; Y.Z. helped with structural analysis; W.Z. and R.H. performed imaging quantitation of human samples; C.H.A.T., C.C.A.H., R.V., P.G., H.M., S.S., and M.B. provided critical insights and discussion; and L.Q. conceived the idea, designed experiments and wrote the manuscript; all authors commented on and approved the manuscript.

ACKNOWLEDGEMENTS

We thank Dr. Richard Wojcikiewicz for the Hrd1 antibody, and members in the Arvan/Qi laboratories for technical assistance and insightful discussions; and the University of Michigan Comprehensive Cancer Center (UMCCC) Tissue Core, Advanced Genomics Core, Imaging Laboratory of Michigan Diabetes Research Center, the Microscopy Core of Biomedical Research Core Facilities and Michigan Center for Materials Characterization for their support. This work is supported by NIH 1R01CA163910 (C.C.A.H.), 1R35GM136422 (Y.Z.), National Natural Science Foundation of China 81620108004 and 81830025 (M.L.), NCATS UL1TR002240 (M.B.), NIH 1R01DK120330, 1R01DK120047, 1R35GM130292 and a pilot grant from George M. O'Brien Kidney Translational Core Center at the University of Michigan P30DK081943 (L.Q.). S.Y is in part supported by Frontiers Science Center for Cell Responses Grant from Nankai University (C029205001). Z.Z is supported by ADA Postdoctoral Fellowship (1-19-PDF-093).

REFERENCES

1. Garg P. A Review of Podocyte Biology. *Am J Nephrol.* 2018;47 Suppl 1:3-13.
2. Shih NY, Li J, Karpitskii V, Nguyen A, Dustin ML, Kanagawa O, Miner JH, and Shaw AS. Congenital nephrotic syndrome in mice lacking CD2-associated protein. *Science.* 1999;286(5438):312-5.

3. Kestila M, Lenkkeri U, Mannikko M, Lamerdin J, McCready P, Putaala H, Ruotsalainen V, Morita T, Nissinen M, Herva R, Kashtan CE, Peltonen L, Holmberg C, Olsen A, and Tryggvason K. Positionally cloned gene for a novel glomerular protein--nephrin--is mutated in congenital nephrotic syndrome. *Mol Cell.* 1998;1(4):575-82.
4. Boute N, Gribouval O, Roselli S, Benessy F, Lee H, Fuchshuber A, Dahan K, Gubler MC, Niaudet P, and Antignac C. NPHS2, encoding the glomerular protein podocin, is mutated in autosomal recessive steroid-resistant nephrotic syndrome. *Nat Genet.* 2000;24(4):349-54.
5. Mollet G, Ratelade J, Boyer O, Muda AO, Morisset L, Lavin TA, Kitzis D, Dallman MJ, Bugeon L, Hubner N, Gubler MC, Antignac C, and Esquivel EL. Podocin inactivation in mature kidneys causes focal segmental glomerulosclerosis and nephrotic syndrome. *J Am Soc Nephrol.* 2009;20(10):2181-9.
6. Chen YM, and Liapis H. Focal segmental glomerulosclerosis: molecular genetics and targeted therapies. *BMC Nephrol.* 2015;16:101.
7. Lenkkeri U, Mannikko M, McCready P, Lamerdin J, Gribouval O, Niaudet PM, Antignac CK, Kashtan CE, Homberg C, Olsen A, Kestila M, and Tryggvason K. Structure of the gene for congenital nephrotic syndrome of the finnish type (NPHS1) and characterization of mutations. *Am J Hum Genet.* 1999;64(1):51-61.
8. Putaala H, Soininen R, Kilpelainen P, Wartiovaara J, and Tryggvason K. The murine nephrin gene is specifically expressed in kidney, brain and pancreas: inactivation of the gene leads to massive proteinuria and neonatal death. *Hum Mol Genet.* 2001;10(1):1-8.
9. Holmberg C, Antikainen M, Ronnholm K, Ala Houhala M, and Jalanko H. Management of congenital nephrotic syndrome of the Finnish type. *Pediatr Nephrol.* 1995;9(1):87-93.
10. Holmberg C, Jalanko H, Koskimies O, Leijala M, Salmela K, Eklund B, and Ahonen J. Renal transplantation in small children with congenital nephrotic syndrome of the Finnish type. *Transplant Proc.* 1991;23(1 Pt 2):1378-9.
11. Park SJ, Kim Y, Yang SM, Henderson MJ, Yang W, Lindahl M, Urano F, and Chen YM. Discovery of endoplasmic reticulum calcium stabilizers to rescue ER-stressed podocytes in nephrotic syndrome. *Proc Natl Acad Sci U S A.* 2019;116(28):14154-63.
12. Jalanko H. Congenital nephrotic syndrome. *Pediatr Nephrol.* 2009;24(11):2121-8.
13. Rantanen M, Palmen T, Patari A, Ahola H, Lehtonen S, Astrom E, Floss T, Vauti F, Wurst W, Ruiz P, Kerjaschki D, and Holthofer H. Nephrin TRAP mice lack slit diaphragms and show fibrotic glomeruli and cystic tubular lesions. *J Am Soc Nephrol.* 2002;13(6):1586-94.
14. Martin CE, and Jones N. Nephrin Signaling in the Podocyte: An Updated View of Signal Regulation at the Slit Diaphragm and Beyond. *Front Endocrinol (Lausanne).* 2018;9:302.
15. Liu L, Done SC, Khoshnoodi J, Bertorello A, Wartiovaara J, Berggren PO, and Tryggvason K. Defective nephrin trafficking caused by missense mutations in the NPHS1 gene: insight into the mechanisms of congenital nephrotic syndrome. *Hum Mol Genet.* 2001;10(23):2637-44.
16. Cybulsky AV. The intersecting roles of endoplasmic reticulum stress, ubiquitin-proteasome system, and autophagy in the pathogenesis of proteinuric kidney disease. *Kidney international.* 2013;84(1):25-33.
17. Cybulsky AV. Endoplasmic reticulum stress, the unfolded protein response and autophagy in kidney diseases. *Nat Rev Nephrol.* 2017;13(11):681-96.
18. Inagi R, Ishimoto Y, and Nangaku M. Proteostasis in endoplasmic reticulum--new mechanisms in kidney disease. *Nat Rev Nephrol.* 2014;10(7):369-78.
19. Inoki K, Mori H, Wang J, Suzuki T, Hong S, Yoshida S, Blattner SM, Ikenoue T, Ruegg MA, Hall MN, Kwiatkowski DJ, Rastaldi MP, Huber TB, Kretzler M, Holzman LB, Wiggins RC, and Guan KL. mTORC1 activation in podocytes is a critical step in the development of diabetic nephropathy in mice. *J Clin Invest.* 2011;121(6):2181-96.

20. Ito N, Nishibori Y, Ito Y, Takagi H, Akimoto Y, Kudo A, Asanuma K, Sai Y, Miyamoto K, Takenaka H, and Yan K. mTORC1 activation triggers the unfolded protein response in podocytes and leads to nephrotic syndrome. *Lab Invest.* 2011;91(11):1584-95.
21. Chen YM, Zhou Y, Go G, Marmerstein JT, Kikkawa Y, and Miner JH. Laminin beta2 gene missense mutation produces endoplasmic reticulum stress in podocytes. *J Am Soc Nephrol.* 2013;24(8):1223-33.
22. Cybulsky AV, Takano T, Papillon J, Bijian K, Guillemette J, and Kennedy CR. Glomerular epithelial cell injury associated with mutant alpha-actinin-4. *Am J Physiol Renal Physiol.* 2009;297(4):F987-95.
23. Pieri M, Stefanou C, Zaravinos A, Erguler K, Stylianou K, Lapathitis G, Karaiskos C, Savva I, Paraskeva R, Dweep H, Sticht C, Anastasiadou N, Zouvani I, Goumenos D, Felekkis K, Saleem M, Voskarides K, Gretz N, and Deltas C. Evidence for activation of the unfolded protein response in collagen IV nephropathies. *J Am Soc Nephrol.* 2014;25(2):260-75.
24. Kaufman DR, Papillon J, Larose L, Iwawaki T, and Cybulsky AV. Deletion of inositol-requiring enzyme-1alpha in podocytes disrupts glomerular capillary integrity and autophagy. *Mol Biol Cell.* 2017;28(12):1636-51.
25. Hassan H, Tian X, Inoue K, Chai N, Liu C, Soda K, Moeckel G, Tufro A, Lee AH, Somlo S, Fedeles S, and Ishibe S. Essential Role of X-Box Binding Protein-1 during Endoplasmic Reticulum Stress in Podocytes. *J Am Soc Nephrol.* 2016;27(4):1055-65.
26. Hartleben B, Godel M, Meyer-Schwesinger C, Liu S, Ulrich T, Kobler S, Wiech T, Grahammer F, Arnold SJ, Lindenmeyer MT, Cohen CD, Pavenstadt H, Kerjaschki D, Mizushima N, Shaw AS, Walz G, and Huber TB. Autophagy influences glomerular disease susceptibility and maintains podocyte homeostasis in aging mice. *J Clin Invest.* 2010;120(4):1084-96.
27. Bhattacharya A, and Qi L. ER-associated degradation in health and disease - from substrate to organism. *J Cell Sci.* 2019;132(23):jcs232850.
28. Hwang J, and Qi L. Quality Control in the Endoplasmic Reticulum: Crosstalk between ERAD and UPR pathways. *Trends Biochem Sci.* 2018;43(8):593-605.
29. Guerriero CJ, and Brodsky JL. The delicate balance between secreted protein folding and endoplasmic reticulum-associated degradation in human physiology. *Physiol Rev.* 2012;92(2):537-76.
30. Mueller B, Lilley BN, and Ploegh HL. SEL1L, the homologue of yeast Hrd3p, is involved in protein dislocation from the mammalian ER. *J Cell Biol.* 2006;175(2):261-70.
31. Mueller B, Klemm EJ, Spooner E, Claessen JH, and Ploegh HL. SEL1L nucleates a protein complex required for dislocation of misfolded glycoproteins. *Proc Natl Acad Sci USA.* 2008;105(34):12325-30.
32. Hampton RY, Gardner RG, and Rine J. Role of 26S proteasome and HRD genes in the degradation of 3-hydroxy-3-methylglutaryl-CoA reductase, an integral endoplasmic reticulum membrane protein. *Mol Biol Cell.* 1996;7(12):2029-44.
33. Plemper RK, Bordallo J, Deak PM, Taxis C, Hitt R, and Wolf DH. Genetic interactions of Hrd3p and Der3p/Hrd1p with Sec61p suggest a retro-translocation complex mediating protein transport for ER degradation. *J Cell Sci.* 1999;112 (Pt 22):4123-34.
34. Qi L, Tsai B, and Arvan P. New Insights into the Physiological Role of Endoplasmic Reticulum-Associated Degradation. *Trends Cell Biol.* 2017;27(6):430-40.
35. Sun S, Shi G, Han X, Francisco AB, Ji Y, Mendonca N, Liu X, Locasale JW, Simpson KW, Duhamel GE, Kersten S, Yates JR, 3rd, Long Q, and Qi L. Sel1L is indispensable for mammalian endoplasmic reticulum-associated degradation, endoplasmic reticulum homeostasis, and survival. *Proc Natl Acad Sci U S A.* 2014;111:E582-91.
36. Fujita H, Yagishita N, Aratani S, Saito-Fujita T, Morota S, Yamano Y, Hansson MJ, Inazu M, Kokuba H, Sudo K, Sato E, Kawahara KI, Nakajima F, Hasegawa D, Higuchi I, Sato T, Araya N, Usui C, Nishioka K, Nakatani Y, Maruyama I, Usui M, Hara N, Uchino H, Elmer

E, Nishioka K, and Nakajima T. The E3 ligase synoviolin controls body weight and mitochondrial biogenesis through negative regulation of PGC-1beta. *EMBO J.* 2015;34(8):1042-55.
37. Shi G, Somlo D, Kim GH, Prescianotto-Baschong C, Sun S, Beuret N, Long Q, Rutishauser J, Arvan P, Spiess M, and Qi L. ER-associated degradation is required for vasopressin prohormone processing and systemic water homeostasis. *J Clin Invest.* 2017;127(10):3897-912.
38. Kim GH, Shi G, Somlo DRM, Haataja L, Soon S, Long Q, Nillni EA, Low MJ, Arvan P, Myers MG, and Qi L. Hypothalamic ER-associated degradation regulates POMC maturation, feeding and age-associated obesity. *J Clin Invest.* 2018;128(3):1125-40.
39. Ji Y, Kim H, Yang L, Sha H, Roman CA, Long Q, and Qi L. The Sel1L-Hrd1 Endoplasmic Reticulum-Associated Degradation Complex Manages a Key Checkpoint in B Cell Development. *Cell reports.* 2016;16(10):2630-40.
40. Sun S, Louri R, Cohen SB, Ji Y, Goodrich JK, Poole AC, Ley RE, Denkers EY, Mcguckin MA, Long Q, Duhamel GE, Simpson KW, and Qi L. Epithelial Sel1L is required for the maintenance of intestinal homeostasis. *Mol Biol Cell.* 2016;27(3):483-90.
41. Bhattacharya A, Sun S, Wang H, Liu M, Long Q, Yin L, Kersten S, Zhang K, and Qi L. Hepatic Sel1L-Hrd1 ER-associated degradation (ERAD) manages FGF21 levels and systemic metabolism via CREBH. *EMBO J.* 2018;37(22):e99277.
42. Shrestha N, Liu T, Ji Y, Reinert RB, Torres M, Li X, Zhang M, Tang CA, Hu CA, Liu C, Naji A, Liu M, Lin JD, Kersten S, Arvan P, and Qi L. Sel1L-Hrd1 ER-associated degradation maintains β cell identity via TGFβ signaling. *J Clin Invest.* 2020;130(7):3499-510.
43. Zhou Z, Torres M, Sha H, Halbrook CJ, Van den Bergh F, Reinert RB, Yamada T, Wang S, Luo Y, Hunter AH, Wang C, Sanderson TH, Liu M, Taylor A, Sesaki H, Lyssiotis CA, Wu J, Kersten S, Beard DA, and Qi L. Endoplasmic reticulum-associated degradation regulates mitochondrial dynamics in brown adipocytes. *Science.* 2020;368:54-60.
44. Wu T, Zhao F, Gao B, Tan C, Yagishita N, Nakajima T, Wong PK, Chapman E, Fang D, and Zhang DD. Hrd1 suppresses Nrf2-mediated cellular protection during liver cirrhosis. *Genes Dev.* 2014;28(7):708-22.
45. Xu Y, Zhao F, Qiu Q, Chen K, Wei J, Kong Q, Gao B, Melo-Cardenas J, Zhang B, Zhang J, Song J, Zhang DD, Zhang J, Fan Y, Li H, and Fang D. The ER membrane-anchored ubiquitin ligase Hrd1 is a positive regulator of T-cell immunity. *Nature communications.* 2016;7:12073.
46. Wei J, Chen L, Li F, Yuan Y, Wang Y, Xia W, Zhang Y, Xu Y, Yang Z, Gao B, Jin C, Melo-Cardenas J, Green RM, Pan H, Wang J, He F, Zhang K, and Fang D. HRD1-ERAD controls production of the hepatokine FGF21 through CREBH polyubiquitination. *EMBO J.* 2018;37(22):e98942.
47. Hu Y, Gao Y, Zhang M, Deng KY, Singh R, Tian Q, Gong Y, Pan Z, Liu Q, Boisclair YR, and Long Q. Endoplasmic Reticulum-Associated Degradation (ERAD) Has a Critical Role in Supporting Glucose-Stimulated Insulin Secretion in Pancreatic beta-Cells. *Diabetes.* 2019;68(4):733-46.
48. Sha H, Sun S, Francisco AB, Ehrhardt N, Xue Z, Liu L, Lawrence P, Mattijssen F, Guber RD, Panhwar MS, Brenna JT, Shi H, Xue B, Kersten S, Bensadoun A, Peterfy M, Long Q, and Qi L. The ER-associated degradation adaptor protein Sel1L regulates LPL secretion and lipid metabolism. *Cell Metab.* 2014;20(3):458-70.
49. Sun S, Shi G, Sha H, Ji Y, Han X, Shu X, Ma H, Inoue T, Gao B, Kim H, Bu P, Guber RD, Shen X, Lee AH, Iwawaki T, Paton AW, Paton JC, Fang D, Tsai B, Yates Iii JR, Wu H, Kersten S, Long Q, Duhamel GE, Simpson KW, and Qi L. IRE1a is an endogenous substrate of endoplasmic-reticulum-associated degradation. *Nat Cell Biol.* 2015;17(12):1546-55.

50. Kato M, Wang M, Chen Z, Bhatt K, Oh HJ, Lanting L, Deshpande S, Jia Y, Lai JY, O'Connor CL, Wu Y, Hodgin JB, Nelson RG, Bitzer M, and Natarajan R. An endoplasmic reticulum stress-regulated lncRNA hosting a microRNA megacluster induces early features of diabetic nephropathy. *Nature communications.* 2016;7:12864.
51. Hodgin JB, Bitzer M, Wickman L, Afshinnia F, Wang SQ, O'Connor C, Yang Y, Meadowbrooke C, Chowdhury M, Kikuchi M, Wiggins JE, and Wiggins RC. Glomerular Aging and Focal Global Glomerulosclerosis: A Podometric Perspective. *J Am Soc Nephrol.* 2015;26(12):3162-78.
52. Menon R, Otto EA, Kokoruda A, Zhou J, Zhang Z, Yoon E, Chen YC, Troyanskaya O, Spence JR, Kretzler M, and Cebrian C. Single-cell analysis of progenitor cell dynamics and lineage specification in the human fetal kidney. *Development.* 2018;145(16).
53. Vashistha N, Neal SE, Singh A, Carroll SM, and Hampton RY. Direct and essential function for Hrd3 in ER-associated degradation. *Proc Natl Acad Sci U S A.* 2016;113(21):5934-9.
54. Gardner RG, Swarbrick GM, Bays NW, Cronin SR, Wilhovsky S, Seelig L, Kim C, and Hampton RY. Endoplasmic reticulum degradation requires lumen to cytosol signaling. Transmembrane control of Hrd1p by Hrd3p. *J Cell Biol.* 2000;151(1):69-82.
55. D'Agati VD, Kaskel FJ, and Falk RJ. Focal segmental glomerulosclerosis. *N Engl J Med.* 2011;365(25):2398-411.
56. Moeller MJ, Sanden SK, Soofi A, Wiggins RC, and Holzman LB. Podocyte-specific expression of cre recombinase in transgenic mice. *Genesis.* 2003;35(1):39-42.
57. Grahammer F, Wigge C, Schell C, Kretz O, Patrakka J, Schneider S, Klose M, Kind J, Arnold SJ, Habermann A, Brauniger R, Rinschen MM, Volker L, Bregenzer A, Rubbenstroth D, Boerries M, Kerjaschki D, Miner JH, Walz G, Benzing T, Fornoni A, Frangakis AS, and Huber TB. A flexible, multilayered protein scaffold maintains the slit in between glomerular podocytes. *JCI Insight.* 2016;1(9):e86177.
58. Verma R, Venkatareddy M, Kalinowski A, Li T, Kukla J, Mollin A, Cara-Fuentes G, Patel SR, and Garg P. Nephrin is necessary for podocyte recovery following injury in an adult mature glomerulus. *PLoS One.* 2018;13(6):e0198013.
59. Ruotsalainen V, Ljungberg P, Wartiovaara J, Lenkkeri U, Kestila M, Jalanko H, Holmberg C, and Tryggvason K. Nephrin is specifically located at the slit diaphragm of glomerular podocytes. *Proc Natl Acad Sci U S A.* 1999;96(14):7962-7.
60. Rodewald R, and Karnovsky MJ. Porous substructure of the glomerular slit diaphragm in the rat and mouse. *J Cell Biol.* 1974;60(2):423-33.
61. Wartiovaara J, Ofverstedt LG, Khoshnoodi J, Zhang J, Makela E, Sandin S, Ruotsalainen V, Cheng RH, Jalanko H, Skoglund U, and Tryggvason K. Nephrin strands contribute to a porous slit diaphragm scaffold as revealed by electron tomography. *J Clin Invest.* 2004;114(10):1475-83.
62. Kurihara H, Anderson JM, Kerjaschki D, and Farquhar MG. The altered glomerular filtration slits seen in puromycin aminonucleoside nephrosis and protamine sulfate-treated rats contain the tight junction protein ZO-1. *Am J Pathol.* 1992;141(4):805-16.
63. Macconi D, Ghilardi M, Bonassi ME, Mohamed EI, Abbate M, Colombi F, Remuzzi G, and Remuzzi A. Effect of angiotensin-converting enzyme inhibition on glomerular basement membrane permeability and distribution of zonula occludens-1 in MWF rats. *J Am Soc Nephrol.* 2000;11(3):477-89.
64. Drozdova T, Papillon J, and Cybulsky AV. Nephrin missense mutations: induction of endoplasmic reticulum stress and cell surface rescue by reduction in chaperone interactions. *Physiol Rep.* 2013;1(4):e00086.
65. Tanigawa S, Islam M, Sharmin S, Naganuma H, Yoshimura Y, Haque F, Era T, Nakazato H, Nakanishi K, Sakuma T, Yamamoto T, Kurihara H, Taguchi A, and Nishinakamura R. Organoids from Nephrotic Disease-Derived iPSCs Identify Impaired NEPHRIN

Localization and Slit Diaphragm Formation in Kidney Podocytes. *Stem Cell Reports.* 2018;11(3):727-40.
66. Yan K, Khoshnoodi J, Ruotsalainen V, and Tryggvason K. N-linked glycosylation is critical for the plasma membrane localization of nephrin. *J Am Soc Nephrol.* 2002;13(5):1385-9.
67. Zheng W, Li Y, Zhang C, Pearce R, Mortuza SM, and Zhang Y. Deep-learning contact-map guided protein structure prediction in CASP13. *Proteins.* 2019;87(12):1149-64.
68. Huang X, Pearce R, and Zhang Y. EvoEF2: Accurate and fast energy function for computational protein design. *Bioinformatics.* 2019;36(4):1135-42.
69. Shrestha N, Reinert RB, and Qi L. Endoplasmic Reticulum Protein Quality Control in beta Cells. *Semin Cell Dev Biol.* 2020;103:59-67.
70. Doublier S, Ruotsalainen V, Salvidio G, Lupia E, Biancone L, Conaldi PG, Reponen P, Tryggvason K, and Camussi G. Nephrin redistribution on podocytes is a potential mechanism for proteinuria in patients with primary acquired nephrotic syndrome. *Am J Pathol.* 2001;158(5):1723-31.
71. Doublier S, Salvidio G, Lupia E, Ruotsalainen V, Verzola D, Deferrari G, and Camussi G. Nephrin expression is reduced in human diabetic nephropathy: evidence for a distinct role for glycated albumin and angiotensin II. *Diabetes.* 2003;52(4):1023-30.
72. Iwawaki T, Akai R, Yamanaka S, and Kohno K. Function of IRE1 alpha in the placenta is essential for placental development and embryonic viability. *Proc Natl Acad Sci USA.* 2009;106(39):16657-62.
73. Saleem MA, O'Hare MJ, Reiser J, Coward RJ, Inward CD, Farren T, Xing CY, Ni L, Mathieson PW, and Mundel P. A conditionally immortalized human podocyte cell line demonstrating nephrin and podocin expression. *J Am Soc Nephrol.* 2002;13(3):630-8.
74. Verma R, Venkatareddy M, Kalinowski A, Patel SR, and Garg P. Integrin Ligation Results in Nephrin Tyrosine Phosphorylation In Vitro. *PLoS One.* 2016;11(2):e0148906.

FIGURES AND FIGURE LEGENDS

Figure 1. SEL1L-HRD1 ERAD is expressed in human podocytes. Representative confocal images of SEL1L (**A**) and HRD1 (**B**) staining in kidneys from healthy humans, co-stained with WT1. Asterisks, WT1 positive podocytes. Arrowheads, distal tubular cells also expressing SEL1L/HRD1. In addition to podocytes, WT1 is also expressed in parietal epithelial cells lining the Bowman's capsule (arrows).

Figure 2. *Sel1L* deficiency in podocytes leads to premature lethality. (A-C) Representative confocal images of Sel1L (**A**) and Hrd1 (**B**) staining in mouse kidneys of 3-week (w)-old $Sel1L^{f/f}$ and $Sel1L^{PodCre}$ mice (n=3 mice each), co-stained with WT1, with quantitation shown in **C** (n=59, 45, 130, 119 podocytes from left to right). Asterisks, WT1 positive podocytes. ***, P<0.001 by two-tailed Student's t test. **(D)** Growth curves of males and females of wildtype $Sel1L^{f/f}$, heterozygous $Sel1L^{PodCre/+}$ and knockout $Sel1L^{PodCre}$ mice. 10-w-old $Ire1\alpha^{PodCre}$ mice were included as a control. *, P<0.05, ***, P<0.001 by One-way ANOVA for each age. **(E-G)** Kaplan-Meier survival analysis for combined genders (**E**), males (**F**) and females (**G**). n, number of mice for each cohort. ***, P<0.0001 by the log-rank test comparing $Sel1L^{PodCre}$ mice with other cohorts. Values represent mean ± SEM.

Figure 3. $Sel1L^{PodCre}$ mice exhibit early-onset renal failure starting at 5 weeks of age. (A) Representative images of kidneys at 3, 5, and 10 week (w)-old $Sel1L^{f/f}$ and $Sel1L^{PodCre}$ mice (n=6 each). **(B-D)** Ratio of albumin/creatinine in the urine **(B)** (n=8 each at 3 w; 8-9 each at 5 w; 8 each at 7 w; 8-9 each at 10 w)**,** serum creatinine **(C)** (n=10, 11 at 3 w; 11, 9 at 5 w; 6, 8 at 7 w; 6, 6 at 10 w) and cholesterol **(D)** (n=10 each at 3 w; 10, 9 at 5 w; 5, 8 at 7 w; 5, 4 at 10 w)**.** 10-w-old $Ire1a^{PodCre}$ mice were included as a control for **C-D** (n=5, 6 mice for C and D). Values represent mean ± SEM. *, P<0.05, **, P<0.01 by two-tailed Student's t test and one-way ANOVA were used for 3-7 and 10 w, respectively. **(E-J)** Representative H&E images of kidney sections from 3- (**E-G**) and 5- (**H-J**) w-old mice (n=3). *, protein casts; #, mesangial cell hyperplasia; black arrows, podocytes; yellow arrowheads, capillary lumen.

Figure 4. Sel1L is required for the formation of slit diaphragm. (A-C) Representative scanning electron microscopy (SEM) images of glomeruli from 3- (**A**, n=9, 10 glomeruli), 5- (**B**, n=12, 16 glomeruli), and 10-w-old (**C**, n=9, 5 glomeruli). Two mice each genotype. CB, cell body of podocytes; PP, primary process; SP, secondary process; FP, foot process. **(D-E)** Representative transmission EM (TEM) images of glomeruli from 3- **(D,** n=3 glomeruli each**)** and 5-w-old **(E,** n=6 glomeruli each) mice. Two mice each genotype. Asterisks indicate mesangial cell hyperplasia; arrows, FP fusion. CL, capillary lumen; US, urinary space; GBM, glomerular basement membrane; Endo, endothelial cells; ER, endoplasmic reticulum. **(F)** Representative TEM images of slit diaphragm (white arrows)**. (G)** Diagram illustrating the key proteins involved in slit diaphragm and ERAD. **(H)** Representative of advanced-SEM images showing slit diaphragm (red arrows) in 5-w-old mice (n=7 glomeruli each). Two mice each genotype.

Figure 5. Sel1L deficiency affects the maturation of nascent nephrin in the ER. (A-E) Representative confocal images of nephrin-KDEL **(A)**, nephrin-ZO1 **(B),** podocin-KDEL **(C),** podocin-ZO1 **(D),** and CD2AP-ZO1 **(E)** in kidney sections of 3-w-old mice (n=3 mice each).

Arrows mark the peri-nuclear localization of nephrin **(A)**, co-localization of nephrin with ZO1 **(B)**, the localization of podocin at slit diaphragm **(C)**, and co-localization of podocin and CD2AP with ZO1 **(D-E)**. Images with artificially enhanced KDEL signal is shown in Figure **S6A**. **(F)** Western blot analysis of nephrin in kidney lysates from 3, 5 and 7-w-old mice, with quantitation of the percent of b form in total nephrin shown in (**G**). n=10 mice each at 3 w; 10, 12 at 5 w; and 4 each at 7 w**.** 7-w-old *Ire1a*^{PodCre} mice were included as a control (n=3), and original data shown in Figure **S7A**. **(H)** Western blot analysis of nephrin in EndoH-treated kidney lysates from 5-w-old mice, with quantitation shown in Figure **S6D** (n=5 mice each group). Values represent mean ± SEM. ***, *P*<0.001 by two-tailed Student's t test (3, 5w) and one-way ANOVA (7w).

Figure 6. Nephrin is an endogenous substrate of ERAD, and in the absence of ERAD, nephrin is retained in the ER and associated with BiP. (A) Western blot analysis following nephrin immunoprecipitation in kidneys from 5-w-old mice, showing the interaction between nephrin and BiP in the absence of ERAD. **(B)** Generation of *HRD1*$^{-/-}$ human podocyte cell line. **(C)** Representative confocal images of nephrin-KDEL staining in human podocytes (n=5, 6 cells for WT and *HRD1*$^{-/-}$). **(D)** Western blot analysis of nephrin in transfected WT and *HRD1*$^{-/-}$ HEK293T cells, digested with or without PNGase F (P) or Endo H (E) with quantitation of the percent of EndoH-resistant (r) and sensitive (s) form shown below. **(E-F)** ^{35}S pulse (30 min)-chase (0, 1, 2, 4 hr) analysis of nascent nephrin protein in HEK293T cells, with quantitation of the percent of *a* form in total nephrin shown in (**F**). **(G)** Western blot analysis of Myc immunoprecipitates in transfected HEK293T cells, treated with or without 10 μM MG132 for 5 hr prior to harvest, showing ERAD-mediated ubiquitination of nephrin. **(H)** Western blot analysis of nephrin protein decay in transfected HEK293T cells treated with brefeldin A and/or cycloheximide (CHX) for indicated time points, with quantitation from 4 independent experiments shown below. **(I)** Western blot analysis of nephrin in transfected WT and *Hrd1*$^{-/-}$ N2a cells under nonreducing or reducing conditions, with quantitation of the level of HMW nephrin normalized to total nephrin from three independent experiments shown below. Data are representative of at least 3 independent experiments. Values represent mean ± SEM. **, *P*<0.01, ***, *P*<0.001 by two-tailed Student's t test.

Figure 7. Nephrin disease mutants are unstable, retained in the ER and targeted for proteasomal degradation by ERAD. (A) Structural modeling of human nephrin showing the domains (Ig and fibronectin, FN) and the location of 6 pathogenic mutations. EvoEF2 (ΔΔG) for each mutant is indicated in blue. (**B-C**) The predicted local structures of WT (upper), I171N (lower, **B**) and G270C (lower, **C**). WT and mutated residues were in green and magenta, respectively. Distance between indicated residues are shown. Arrows, disulfide bond. (**D-E**) Western blot analysis of WT and mutant nephrin proteins in transfected HEK293T cells, showing nephrin mutants running as the *b* form on SDS-PAGE. Quantitation shown in (**E**). (**F**) Western blot analysis following EndoH digestion in HEK293T cells transfected with WT or mutant nephrin. (**G-H**) Western blot analysis of WT or mutant nephrin in transfected HEK293T cells treated with CHX for 4 h, with quantitation shown in (**H**). Values represent mean ± SEM. Data are representative of at least 2 independent experiments. *, *P*<0.05 by two-tailed Student's t test.

Figure 8. ERAD of disease mutants attenuates their pathogenicity towards wildtype allele. (A) Western blot analysis of high molecular weight (HMW) and monomer nephrin of WT and mutants under non-reducing and reducing conditions in transfected wildtype and *HRD1*$^{-/-}$ HEK293T cells. **(B-C)** Western blot analysis of NP40-soluble (**B**) and -insoluble fractions (**C**) in transfected wildtype and *HRD1*$^{-/-}$ HEK293T cells, showing increased formation of HMW and insoluble nephrin aggregates in *HRD1*$^{-/-}$ HEK293T cells for both WT and mutant nephrin. **(D)** Western blot analysis of nephrin HMW aggregation in HEK293T cells transfected with different combination of Myc-WT nephrin and nephrin mutants under non-reducing conditions, with quantitation of HMW nephrin from one representative experiment shown below. **(E-F)** Western blot analysis of Myc-WT and Flag-mutant nephrin in HEK293T cells transfected with different combinations of Myc-WT nephrin and Flag-mutant nephrin at 1:1 or 1:3 ratio. Quantitation of % *a* form WT nephrin in total WT nephrin shown in (**F**), showing decreased percent of *a* form WT nephrin in *HRD1*$^{-/-}$ HEK293T (upon co-transfection of an increased amount of mutant nephrin) when compared to that in WT HEK293T cells**.** Values represent mean ± SEM. Data are representative of at least 2 independent experiments.

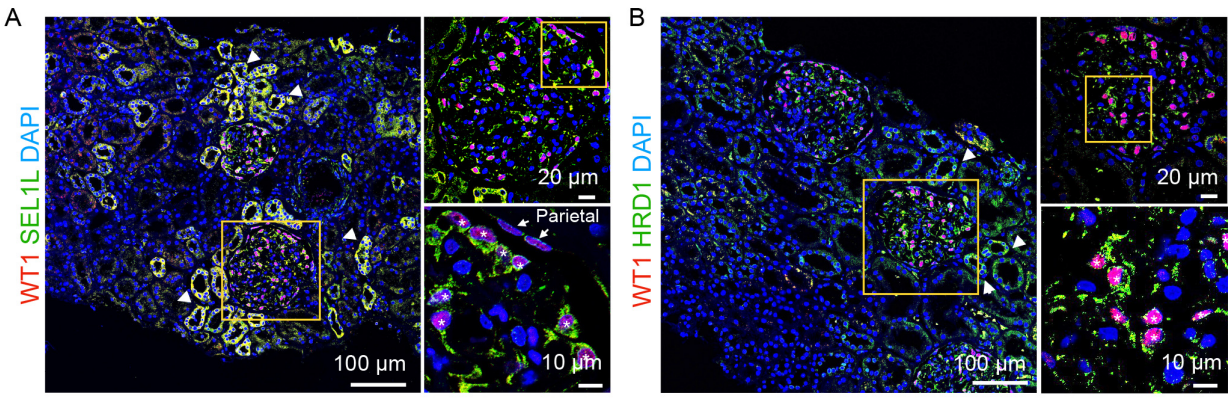

Figure 1. SEL1L-HRD1 ERAD is expressed in human podocytes. Representative confocal images of SEL1L (**A**) and HRD1 (**B**) staining in kidneys from healthy humans, co-stained with WT1. Asterisks, WT1 positive podocytes. Arrowheads, distal tubular cells also expressing SEL1L/HRD1. In addition to podocytes, WT1 is also expressed in parietal epithelial cells lining the Bowman's capsule (arrows).

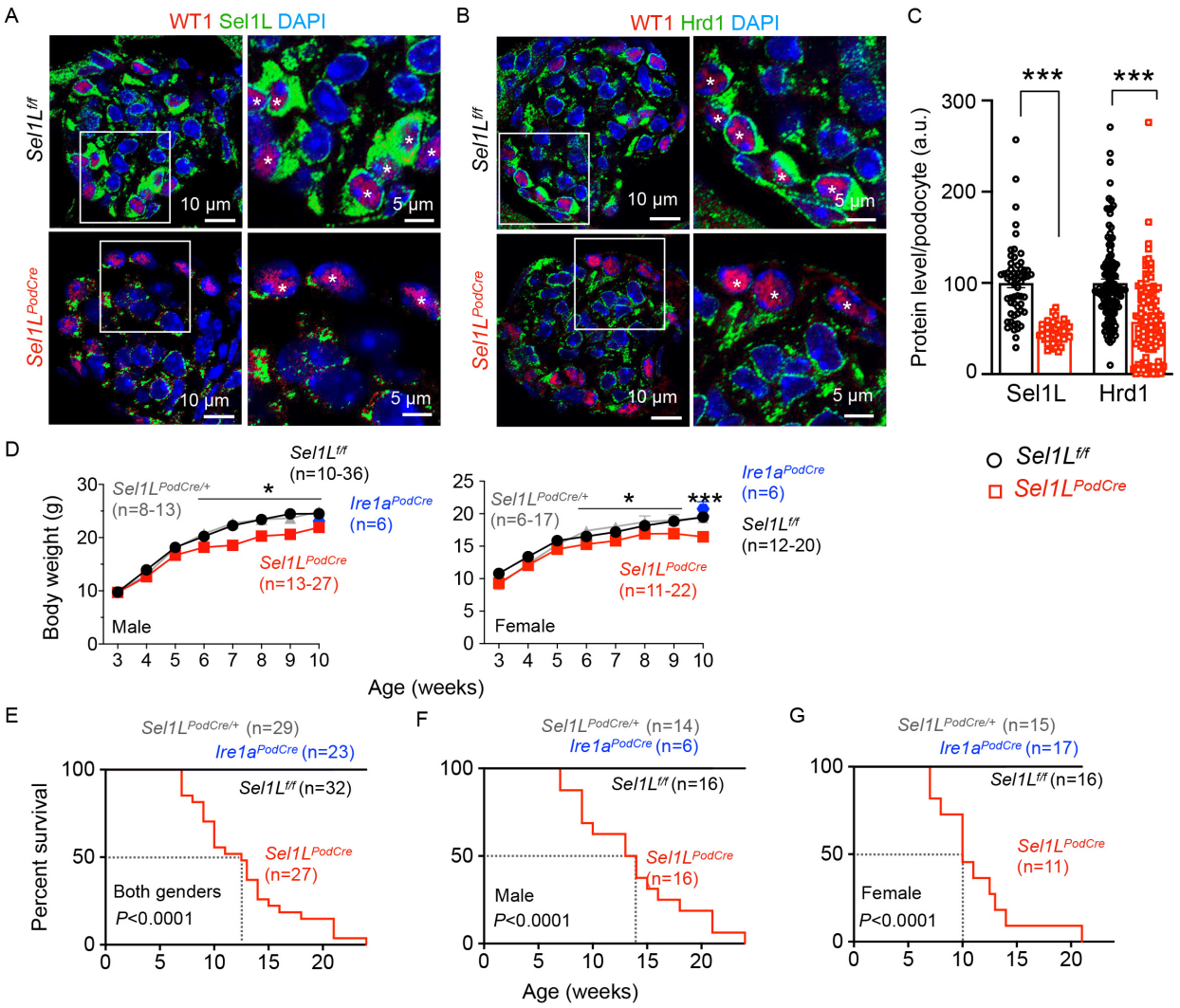

Figure 2. *Sel1L* deficiency in podocytes leads to premature lethality. (A-C) Representative confocal images of Sel1L (**A**) and Hrd1 (**B**) staining in mouse kidneys of 3-week (w)-old *Sel1L*$^{f/f}$ and *Sel1L*^{PodCre} mice (n=3 mice each), co-stained with WT1, with quantitation shown in **C** (n=59, 45, 130, 119 podocytes from left to right). Asterisks, WT1 positive podocytes. ***, *P*<0.001 by two-tailed Student's t test. **(D)** Growth curves of males and females of wildtype *Sel1L*$^{f/f}$, heterozygous *Sel1L*$^{PodCre/+}$ and knockout *Sel1L*^{PodCre} mice. 10-w-old *Ire1a*^{PodCre} mice were included as a control. *, *P*<0.05, ***, *P*<0.001 by One-way ANOVA for each age. **(E-G)** Kaplan-Meier survival analysis for combined genders (**E**), males (**F**) and females (**G**). n, number of mice for each cohort. ***, *P*<0.0001 by the log-rank test comparing *Sel1L*^{PodCre} mice with other cohorts. Values represent mean ± SEM.

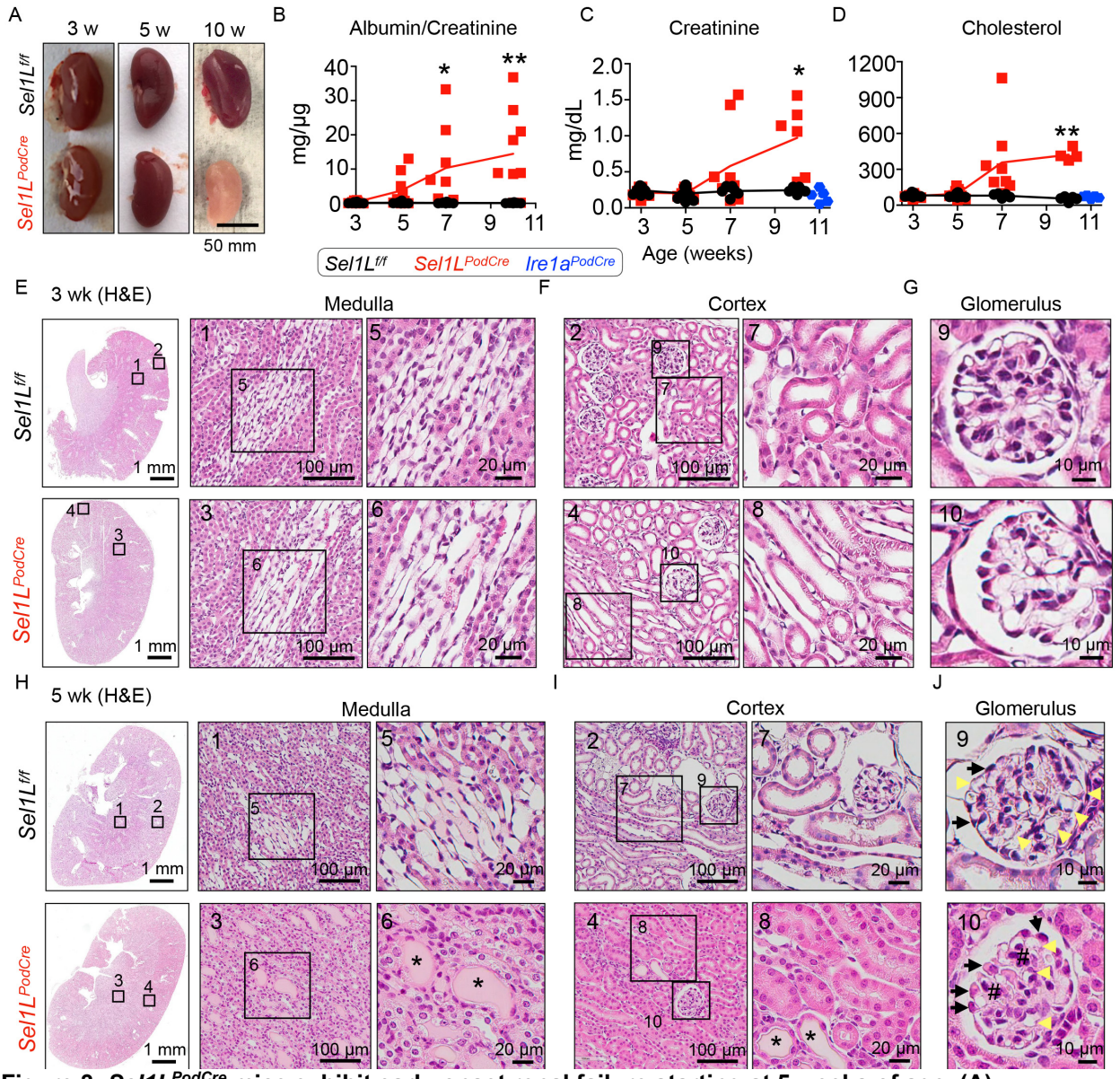

Figure 3. *Sel1L*^{PodCre} mice exhibit early-onset renal failure starting at 5 weeks of age. (A) Representative images of kidneys at 3, 5, and 10 week (w)-old *Sel1L*$^{f/f}$ and *Sel1L*^{PodCre} mice (n=6 each). **(B-D)** Ratio of albumin/creatinine in the urine **(B)** (n=8 each at 3 w; 8-9 each at 5 w; 8 each at 7 w; 8-9 each at 10 w), serum creatinine **(C)** (n=10, 11 at 3 w; 11, 9 at 5 w; 6, 8 at 7 w; 6, 6 at 10 w) and cholesterol **(D)** (n=10 each at 3 w; 10, 9 at 5 w; 5, 8 at 7 w; 5, 4 at 10 w). 10-w-old *Ire1a*^{PodCre} mice were included as a control for **C-D** (n=5, 6 mice for C and D). Values represent mean ± SEM. *, $P<0.05$, **, $P<0.01$ by two-tailed Student's t test and one-way ANOVA were used for 3-7 and 10 w, respectively. **(E-J)** Representative H&E images of kidney sections from 3- (**E-G**) and 5- (**H-J**) w-old mice (n=3). *, protein casts; #, mesangial cell hyperplasia; black arrows, podocytes; yellow arrowheads, capillary lumen.

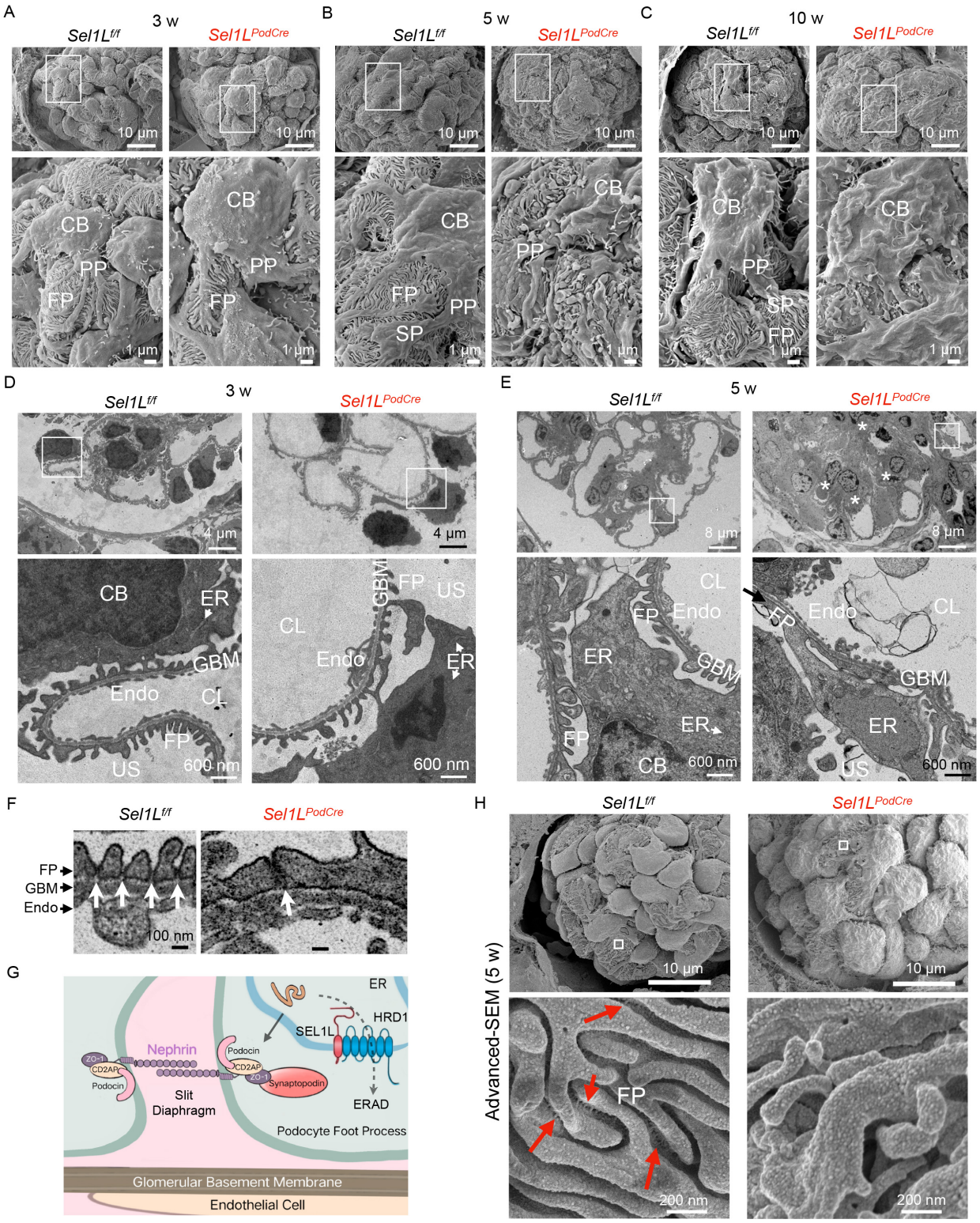

Figure 4. Sel1L is required for the formation of slit diaphragm. (A-C) Representative scanning electron microscopy (SEM) images of glomeruli from 3- (**A**, n=9, 10 glomeruli), 5- (**B**, n=12, 16 glomeruli), and 10-w-old (**C**, n=9, 5 glomeruli). Two mice each genotype. CB, cell body of podocytes; PP, primary process; SP, secondary process; FP, foot process. **(D-E)** Representative transmission EM (TEM) images

of glomeruli from 3- **(D,** n=3 glomeruli each**)** and 5-w-old **(E,** n=6 glomeruli each) mice. Two mice each genotype. Asterisks indicate mesangial cell hyperplasia; arrows, FP fusion. CL, capillary lumen; US, urinary space; GBM, glomerular basement membrane; Endo, endothelial cells; ER, endoplasmic reticulum. **(F)** Representative TEM images of slit diaphragm (white arrows)**. (G)** Diagram illustrating the key proteins involved in slit diaphragm and ERAD. **(H)** Representative of advanced-SEM images showing slit diaphragm (red arrows) in 5-w-old mice (n=7 glomeruli each). Two mice each genotype.

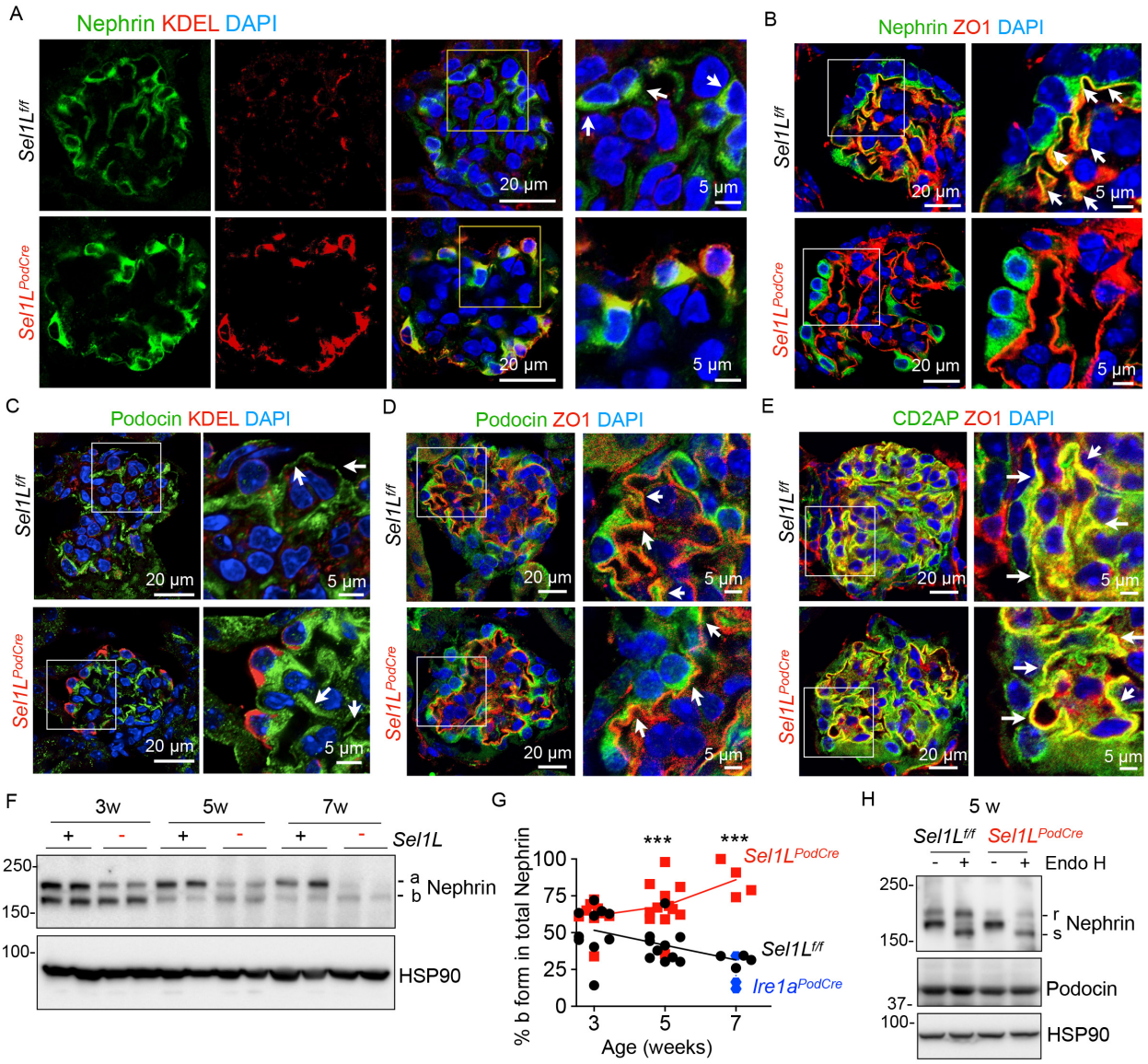

Figure 5. Sel1L deficiency affects the maturation of nascent nephrin in the ER. (A-E) Representative confocal images of nephrin-KDEL **(A)**, nephrin-ZO1 **(B),** podocin-KDEL **(C),** podocin-ZO1 **(D),** and CD2AP-ZO1 **(E)** in kidney sections of 3-w-old mice (*n*=3 mice each). Arrows mark the peri-nuclear localization of nephrin **(A)**, co-localization of nephrin with ZO1 **(B)**, the localization of podocin at slit diaphragm **(C)**, and co-localization of podocin and CD2AP with ZO1 **(D-E)**. Images with artificially enhanced KDEL signal is shown in Figure **S6A**. **(F)** Western blot analysis of nephrin in kidney lysates from 3, 5 and 7-w-old mice, with quantitation of the percent of b form in total nephrin shown in (**G**). n=10 mice each at 3 w; 10, 12 at 5 w; and 4 each at 7 w**.** 7-w-old *Ire1a*^{PodCre} mice were included as a control (n=3), and original data shown in Figure **S7A**. **(H)** Western blot analysis of nephrin in EndoH-treated kidney lysates from 5-w-old mice, with quantitation shown in Figure **S6D** (n=5 mice each group). Values represent mean ± SEM. ***, *P*<0.001 by two-tailed Student's t test (3, 5w) and one-way ANOVA (7w).

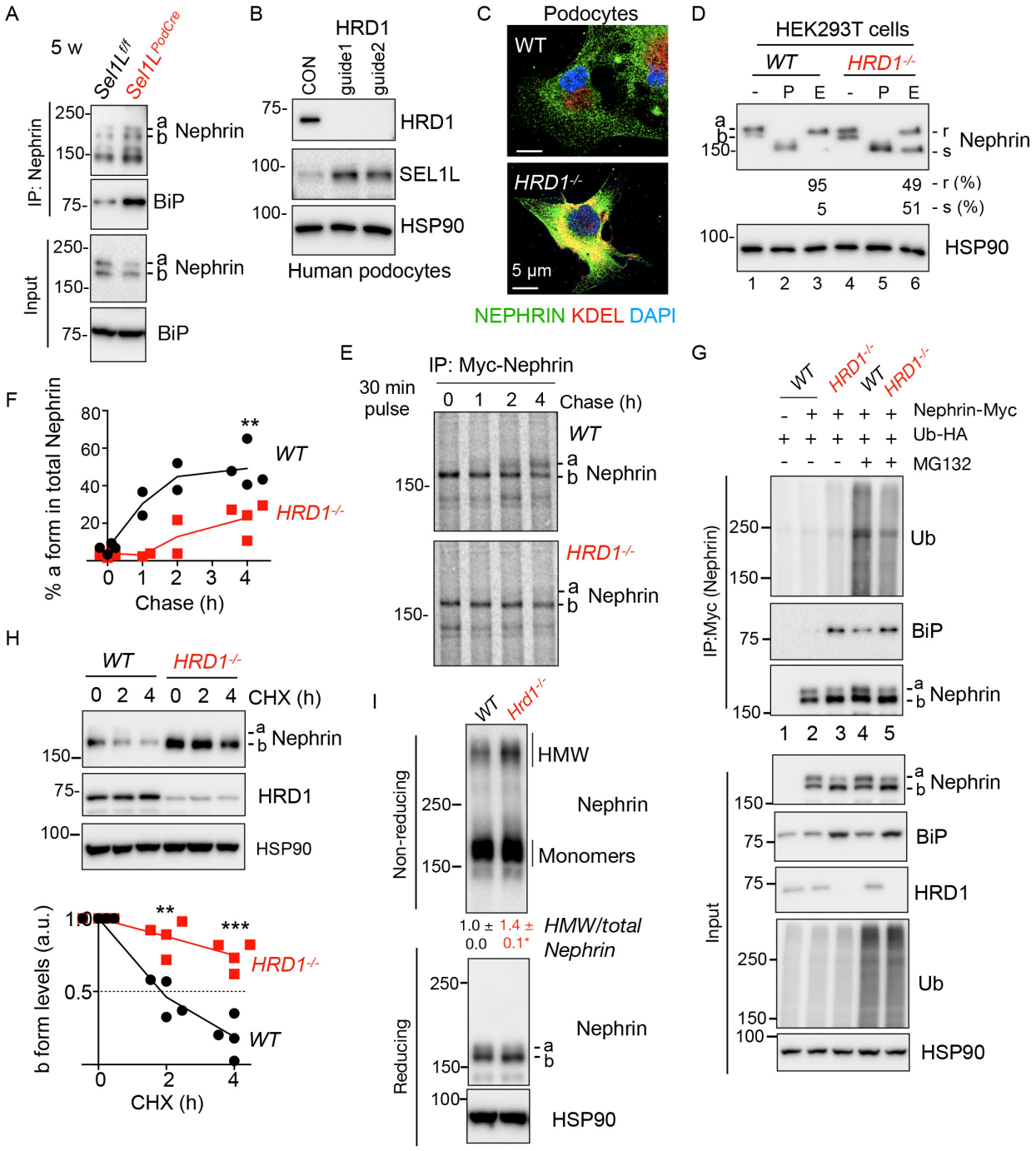

Figure 6. Nephrin is an endogenous substrate of ERAD, and in the absence of ERAD, nephrin is retained in the ER and associated with BiP. (A) Western blot analysis following nephrin immunoprecipitation in kidneys from 5-w-old mice, showing the interaction between nephrin and BiP in the absence of ERAD. **(B)** Generation of *HRD1*$^{-/-}$ human podocyte cell line. **(C)** Representative confocal images of nephrin-KDEL staining in human podocytes (n=5, 6 cells for WT and *HRD1*$^{-/-}$). **(D)** Western blot analysis of nephrin in transfected WT and *HRD1*$^{-/-}$ HEK293T cells, digested with or without PNGase F (P) or Endo H (E) with quantitation of the percent of EndoH-resistant (r) and sensitive (s) form shown below. **(E-F)** ^{35}S pulse (30 min)-chase (0, 1, 2, 4 hr) analysis of nascent nephrin protein in HEK293T cells, with quantitation of the percent of *a* form in total nephrin shown in (**F**). **(G)** Western blot analysis of Myc immunoprecipitates in transfected HEK293T cells, treated with or without 10 μM MG132 for 5 hr prior to

harvest, showing ERAD-mediated ubiquitination of nephrin. **(H)** Western blot analysis of nephrin protein decay in transfected HEK293T cells treated with brefeldin A and/or cycloheximide (CHX) for indicated time points, with quantitation from 4 independent experiments shown below. **(I)** Western blot analysis of nephrin in transfected WT and *Hrd1*$^{-/-}$ N2a cells under nonreducing or reducing conditions, with quantitation of the level of HMW nephrin normalized to total nephrin from three independent experiments shown below. Data are representative of at least 3 independent experiments. Values represent mean ± SEM. **, $P<0.01$, ***, $P<0.001$ by two-tailed Student's t test.

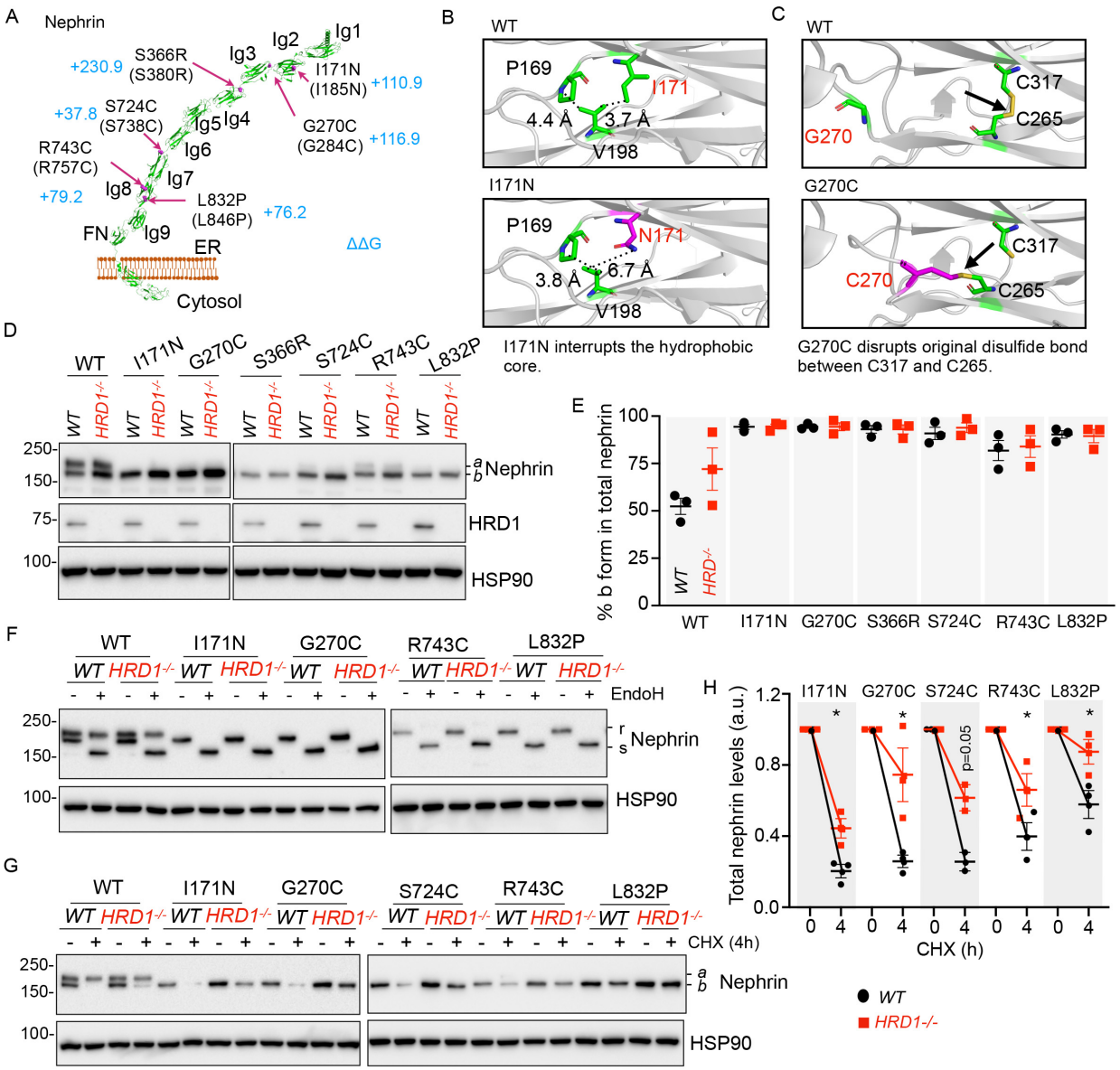

Figure 7. Nephrin disease mutants are unstable, retained in the ER and targeted for proteasomal degradation by ERAD. (A) Structural modeling of human nephrin showing the domains (Ig and fibronectin, FN) and the location of 6 pathogenic mutations. EvoEF2 (ΔΔG) for each mutant is indicated in blue. (**B-C**) The predicted local structures of WT (upper), I171N (lower, **B**) and G270C (lower, **C**). WT and mutated residues were in green and magenta, respectively. Distance between indicated residues are shown. Arrows, disulfide bond. (**D-E**) Western blot analysis of WT and mutant nephrin proteins in transfected HEK293T cells, showing nephrin mutants running as the *b* form on SDS-PAGE. Quantitation shown in (**E**). (**F**) Western blot analysis following EndoH digestion in HEK293T cells transfected with WT or mutant nephrin. (**G-H**) Western blot analysis of WT or mutant nephrin in transfected HEK293T cells treated with CHX for 4 h, with quantitation shown in (**H**). Values represent mean ± SEM. Data are representative of at least 2 independent experiments. *, *P*<0.05 by two-tailed Student's t test.

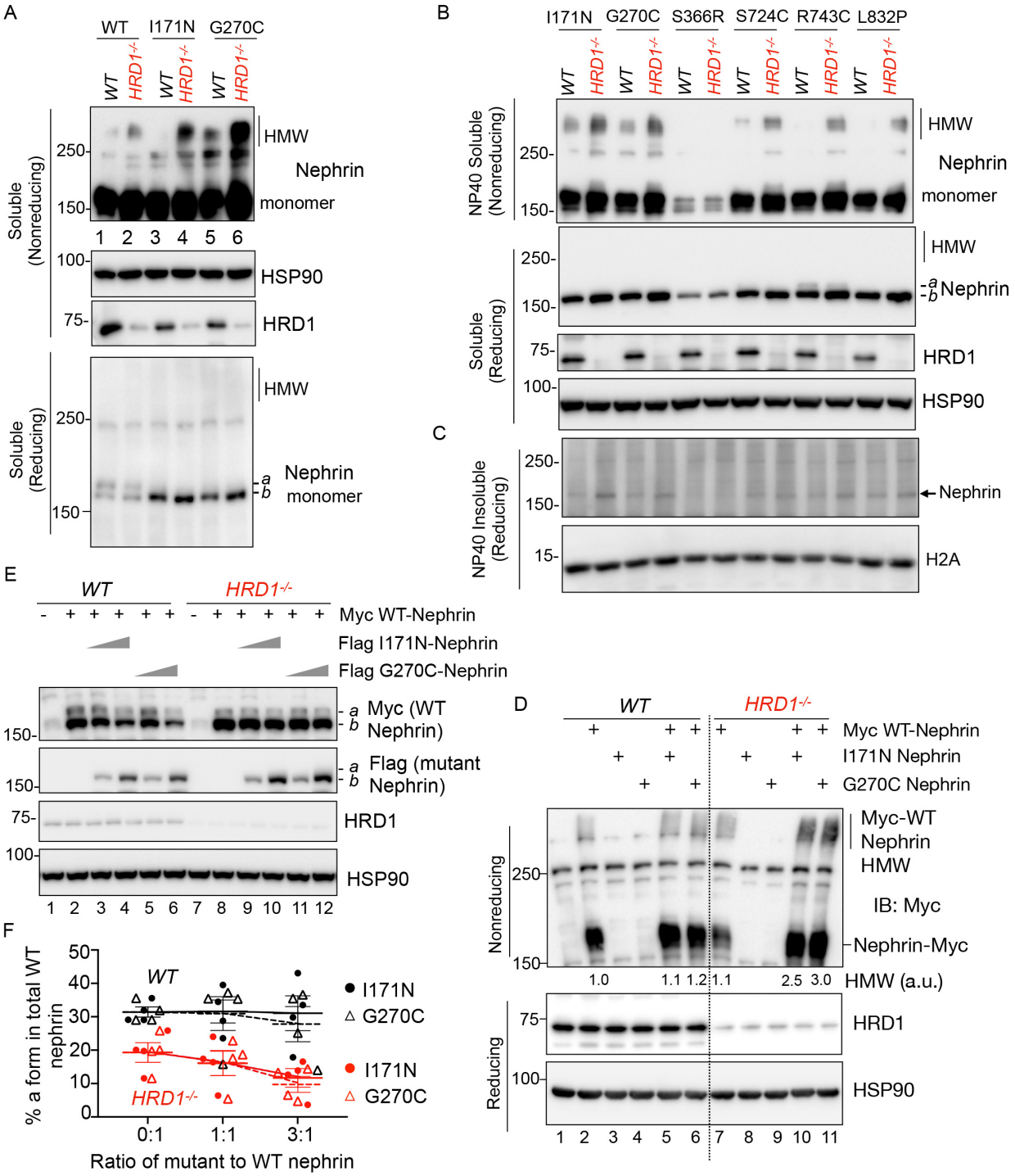

Figure 8. ERAD of disease mutants attenuates their pathogenicity towards wildtype allele. (A) Western blot analysis of high molecular weight (HMW) and monomer nephrin of WT and mutants under non-reducing and reducing conditions in transfected wildtype and *HRD1*$^{-/-}$ HEK293T cells. **(B-C)** Western blot analysis of NP40-soluble (**B**) and -insoluble fractions (**C**) in transfected wildtype and *HRD1*$^{-/-}$ HEK293T cells, showing increased formation of HMW and insoluble nephrin aggregates in *HRD1*$^{-/-}$ HEK293T cells for both WT and mutant nephrin. **(D)** Western blot analysis of nephrin HMW aggregation in HEK293T cells transfected with different combination of Myc-WT nephrin and nephrin mutants under non-reducing conditions, with quantitation of HMW nephrin from one representative experiment shown below. **(E-F)** Western blot analysis of Myc-WT and Flag-mutant nephrin in HEK293T cells transfected with

different combinations of Myc-WT nephrin and Flag-mutant nephrin at 1:1 or 1:3 ratio. Quantitation of % *a* form WT nephrin in total WT nephrin shown in (**F**), showing decreased percent of *a* form WT nephrin in *HRD1*$^{-/-}$ HEK293T (upon co-transfection of an increased amount of mutant nephrin) when compared to that in WT HEK293T cells**.** Values represent mean ± SEM. Data are representative of at least 2 independent experiments.